Axion Dark Matter Photon Conversion

Masaki, Emi

(Degree)
博士（理学）

(Date of Degree)
2021-03-25

(Date of Publication)
2022-03-01

(Resource Type)
doctoral thesis

(Report Number)
甲第8003号

(URL)
https://hdl.handle.net/20.500.14094/D1008003

Doctoral Dissertation

Axion Dark Matter Photon Conversion

(アクシオン暗黒物質の転換現象)

March 2021

Graduate School of Science, Kobe University

Emi Masaki

(正木 愛美)

Abstract

A coherently oscillating axion field is one of the dark matter candidates. Photons propagating in the axion dark matter obey the Mathieu equation, and its solutions could be unstable depending on parameters. This is known as the parametric resonance. In the Universe, there also exist magnetic fields, and they induce the axion photon conversion; that is, axions and photons repeat mixing while propagating. Effects on observation of the axion photon conversion have been investigated in various situations.

In this thesis, we study the axion photon conversion in the situation where axions contribute to the energy density of our Universe as the dark matter. First, we organize the fundamental equations of our system, which contain both the conventional conversion terms and the Mathieu type terms. Then, by using numerical calculation, we classify parameters in the fundamental equations into those which make the solution stable and unstable. As a result, we find not only the unstable condition, which is known in the case of the conventional Mathieu equation, but also another unstable condition specific to our system. Moreover, we derive the width of the unstable band analytically and show how the presence of the magnetic field in the background affects the instability conditions. This is useful when thinking about whether there is a physical system where the conversion and the resonance can be important at the same time.

Contents

Chapter 1

Introduction

1.1 Overview

Our Universe is magnetized everywhere [1, 2]. The existence of magnetic fields with the strength $\sim 10^{-6}\,\mathrm{G}$ in galaxies and galaxy clusters has long been known through observations, *e.g.,* synchrotron emission, Faraday rotation, and so on [3]. Compact objects have considerably strong magnetic fields: white dwarf $10^3 - 10^9\,\mathrm{G}$ [4] and neutron star $10^8 - 10^{15}\,\mathrm{G}$ [5]. In addition, the surprising fact becomes evident; that is, magnetic fields also exist in regions called **void**, where no galaxies exist. The γ-ray measurements give the lower limit for these intergalactic magnetic fields: $\gtrsim 10^{-16}\,\mathrm{G}$ [6, 7]. As described, observations confirm that the magnetic fields are ubiquitous. However, the origin of these magnetic fields in the Universe is still a contentious issue. There is an astrophysical process of amplifying and maintaining magnetic fields, but this mechanism cannot create magnetic fields from scratch. It is thought that the magnetic fields observed today are the result of the amplification of magnetic field "seeds," which have been generated in other processes. There are relatively few opportunities for void magnetic fields to be disturbed by astrophysical processes, so it is expected that they keep the situation at the time of generation. Various theories which try to explain the genesis of seed fields have been proposed so far, and they can be roughly divided into two types. One is the astrophysical origin, and the other is the primordial origin. The former assumes that the magnetic fields are ejected from the astronomical object within the galaxy through some processes; thus, the distribution of magnetic fields might be random. On the other hand, in the latter case, there should be coherence over the cosmological distances, and the helicity of magnetic fields might be non-zero. Understanding the magnetic field's configuration may hold the key to the clarification of magnetogenesis.

In the presence of magnetic fields, it is known that axions and photons can mix with each other [8, 9]. The axion is originally introduced to remove a blemish in the quantum chromodynamics [10–13]. It is a pseudo-Nambu Goldstone boson associated with a spontaneous symmetry breaking of a new global symmetry $\mathrm{U}(1)_{\mathrm{PQ}}$. This original axion is characterized by a single parameter f_a, which is the symmetry breaking energy scale. There is a relation between the value of f_a and its mass. In addition to this original axion, the string theory also predicts similar scalar particles, axionlike particles [14, 15]. They can not necessarily solve the problem which the quantum chromodynamics has,

and its mass is an independent parameter by itself. Therefore, the parameter space of axionlike particles is broader than that of the original one. Throughout this thesis, we simply use a word "axion" for both of them unless otherwise noted. This is because what is important in considering the conversion is the existence of such scalar particles. Once we assume their existence, the difference between them is nothing more than the difference in possible values of parameters. The mixing of photons with such theoretically predicted particles can affect electromagnetic observations. For example, it was pointed out that the result of dimming supernovae could be reproduced by considering the effect of the conversion [16–20]. The conversion can also make high energy photons more transparent [21–30]. Conversion phenomena between axions and photons can also affect the polarization of photons [31–42]. Summarizing the above, the axion photon conversion has the potential for various astrophysical and cosmological consequences.

Axions are generating considerable interest as a dark matter candidate too. In other words, there is a possibility that coherent oscillations of axions make up for the energy density of the dark matter. Behind this, as one of the factors, we can mention the fact that no indication of weakly interacting massive particles (**WIMP**s), which was considered to be an influential candidate, has been given from the LHC search. Of course, it may be too hasty to dismiss the possibility of WIMP dark matter, but it is also important to explore other possibilities. For this reason, scientists make expectations for axions higher. Axions are also well motivated as the beyond standard model and have the potential to give rich phenomena in the history of the Universe. Even better, axions have wide untouched parameter space, and new detection methods targeting such parameters are being proposed one after another. Although it is well known that the cold dark matter scenario can describe the cosmological scale observation, the small scale structure has not yet been fully clarified. It is still a matter of debate in terms of both theoretical predictions and observations. There might be a possibility that the ultralight axion whose mass is around $\sim 10^{-22}\,\mathrm{eV}$ is favored due to its feature of suppressing small scale structures.

In light of the above, we have studied conversion phenomena in the presence of both magnetic fields and oscillating axions in the background. As a first step before considering effects on the observation, we mainly study the stability of such a conversion system. What we have studied and derived in this thesis are summarized as follows.

1. We have prepared the fundamental equations of the axion dark matter photon conversion. The originality of this study lies in the fact that we have dealt with the conversion and the parametric resonance at the same time.

2. The numerical approach, which is known in the case of the parametric resonance described by the Mathieu equation, has been applied to our system. As a result, we have found the peculiar unstable condition which does not appear in the conventional Mathieu equation. The numerical results show regions which make the solution stable and unstable on the parameter plane.

3. We have analytically derived the location and the width of the unstable region by treating parameters as small quantities. This is useful when we consider a concrete physical setup and an impact on the observation.

4. We have briefly discussed whether there is a system in which the conversion and the parametric resonance are important at the same time. It has turned out that, in naive situations, it is difficult to observe the signals specific to our system. We leave the following points as future works; that is, we examine how we can devise a physical setup to obtain an observable signal and what information can be extracted from the signal.

Throughout this thesis, we adopt $\hbar = c = 1$, natural Lorentz-Heaviside units, mostly positive metric, and $\varepsilon_{0123} = +1$.

1.2 Structure of This Thesis

• Chap. 1 : Introduction

As an introduction, we provide an overview and the composition of this thesis.

• Chap. 2 : Review Part about Axions

The knowledge about axions is summarized, focusing on what is necessary for understanding the main part, Chap. 4. In Sec. 2.1, We mention the fact that there are two different possibilities of the theoretical background to axions, namely the QCD axion and axionlike particles, and the common feature of them is shown. In Sec. 2.2, we summarize parameters which characterize axions. In Sec. 2.3, the axion photon coupling is introduced. This is the key interaction for our main part, and the detection of axion is frequently based on this interaction. In Sec. 2.4, we focus on the aspect that the axion is a candidate for the dark matter. After looking at the general properties of the dark matter, which are indicated by observations, we show that axions, in fact, have the appropriate properties. The observation of the dark matter near the solar system is also mentioned. In Sec. 2.5, representative axion searches and constraints for the axion photon coupling are shown.

• Chap. 3 : Review Part about Conversion Phenomena

This chapter is an overview of the conventional conversion phenomenon between axions and photons in the presence of the background magnetic field. In Sec. 3.1, the equations of motion for the system under consideration are derived, and linearized equations of motion are given in Sec. 3.2. In Sec. 3.3, a commonly used expression is shown by performing the further transformation. Some effects which give effective mass to photons are introduced in Sec. 3.4, and the conversion probability is derived in Sec. 3.5. In Sec. 3.6, effects on the polarization of photons due to axion photon conversion are explained. In Sec. 3.7, as one example, we treat the physical application of the axion photon conversion. The magnetic fields which exist in the Universe are modeled in two ways. We see how the polarization of photons is affected by the conversion phenomena in each case.

- **Chap. 4 : Main Part**

The main topic based on Ref. [43] is given in this chapter. We consider the conversion in the situation where there is not only a static magnetic field but also an oscillating axion in the background. In Sec. 4.1, we solve background equations and derive perturbative equations in Sec. 4.2. In Sec. 4.3, by using numerical calculation, we classify the parameters included in perturbative equations into stable and unstable sets. At the same time, we show analytical results in advance, which are derived in Sec. 4.4. In Sec. 4.5, the physical applications of the system treated in this thesis are briefly discussed.

- **Chap. 5 : Conclusion**

We draw our conclusions in the final chapter.

- **Appendix**

For a better understanding of the main part, Chap. 4, we have included two appendices. In Appx. A, we review the general knowledge about the Mathieu equation, which describes the parametric resonance. In Appx. B, we present concrete expressions which were not able to be covered in the text.

Chapter 2

Axions

In this chapter, we summarized the minimum knowledge about axion with reference to, *e.g.,* Refs. [44–47] and references, which are mentioned at each point. Throughout this thesis, unless otherwise noted, we simply use a word "axion" for both QCD axion and axionlike particles. As far as the main topic, conversion phenomena, is concerned, the difference between them is nothing more than the difference in possible values of parameters.

2.1 QCD axion and ALPs

The axion originated as the resolution of the **strong CP problem**: why is the CP symmetry conserved in the quantum chromodynamics (**QCD**)? R.Peccei and H.Quinn tackled this problem by postulating a new $\mathrm{U}(1)_{\mathrm{PQ}}$ global symmetry (**PQ symmetry**) [10, 11]. Spontaneous breaking of this symmetry $\mathrm{U}(1)_{\mathrm{PQ}}$ gives rise to a pseudo-Nambu-Goldstone boson, so-called **QCD axion** [12, 13]. The symmetry breaking energy scale f_a is called **decay constant**.

It is known that the string theory has the potential to provide many pseudoscalar particles in the low-energy four dimensional limit, so-called axionlike particles (**ALPs**) [14, 15]. They are not necessarily the resolution for the strong CP problem.

QCD axion and ALPs share the basic feature. They arise as a massless particle with a shift symmetry,

$$a \to a + \text{const.} \ , \tag{2.1.1}$$

where a is the axion. Due to the non-perturbative quantum effects (*e.g.,* instanton), the axion obtain the periodic potential [1],

$$V(a) = \Lambda^4 \left[1 - \cos\left(\frac{a}{f_a} \right) \right] \ , \tag{2.1.2}$$

where Λ is the energy scale which the non-perturbative effects turn on. Along with this potential, the shift symmetry becomes the discrete shift symmetry,

$$a \to a + 2\pi f_a. \tag{2.1.3}$$

[1] This potential expression is not unique but a qualitative one. In order to get a concrete form of $V(a)$, we need detailed knowledge about the non-perturbative effect.

Provided that there are only small displacements from the potential minimum, $a \ll f_a$, we can expand the potential Eq. (2.1.2)

$$V(a) \simeq \Lambda^4 \left[1 - 1 + \frac{1}{2}\left(\frac{a}{f_a}\right)^2 \right] = \frac{1}{2}\left(\frac{\Lambda^2}{f_a}\right)^2 a^2 \ . \tag{2.1.4}$$

Thus, axion obtains a mass:

$$m_a \sim \frac{\Lambda^2}{f_a} \ . \tag{2.1.5}$$

2.2 Parameters which Characterize Axions

The physical properties of the QCD axion are essentially determined by the decay constant f_a. The mass of axion induced by QCD instanton is calculated in Refs. [12,48,49]. Here, we quote the result,

$$m_{a,\mathrm{QCD}} \simeq 6 \times 10^{-10}\,\mathrm{eV}\left(\frac{10^{16}\,\mathrm{GeV}}{f_a}\right) \ . \tag{2.2.1}$$

In the case of QCD axion, there is a relation between mass $m_{a,\mathrm{QCD}}$ and decay constant f_a. In the original model, the electroweak scale $f_a \simeq 250\,\mathrm{GeV}$ was assumed [44, 50], but this parameter was ruled out immediately by experiments. Accordingly, nowadays, it is considered that f_a is much larger. However, the QCD axion cannot be lighter than $10^{-13}\,\mathrm{eV}$ from the point of view that the decay constant f_a will never exceed the Planck scale no matter how big it is. Light QCD axions with mass range $6\times10^{-13}\,\mathrm{eV} < m_{a,\mathrm{QCD}} < 2 \times 10^{-11}\,\mathrm{eV}$ are excluded by black hole superradiance [51, 52]. There are upper bounds on the mass $m_{a,\mathrm{QCD}}$ from stellar evolution, *e.g.,* globular clusters [45, 53, 54] and the supernova SN1987A [45, 55–57]. To sum up, we assume roughly

$$10^{-11}\,\mathrm{eV} \lesssim m_{a,\mathrm{QCD}} \lesssim 10^{-2}\,\mathrm{eV} \ , \tag{2.2.2}$$

as a mass range for QCD axion. At the same time, we assume

$$10^{9}\,\mathrm{GeV} \lesssim f_a \lesssim 10^{17}\,\mathrm{GeV} \ . \tag{2.2.3}$$

Since the interaction strengths are inversely proportional to f_a, axion has extremely weak interactions with other particles, so it is called the **invisible axion**. In the case of QCD axion, the energy scale Λ is given by $\Lambda^2 \sim \Lambda_{\mathrm{QCD}}^{3/2}\sqrt{m_u}$ with $\Lambda_{\mathrm{QCD}} \simeq 200\mathrm{MeV}$ and up quark mass m_u [44].

On the other hand, in the case of ALPs, there is no such relationship as Eq. (2.2.1), and its mass $m_{a,\mathrm{ALP}}$ is an independent parameter by itself [14, 15, 44]. The energy scale Λ can be written as follows:

$$\Lambda = \mu e^{-S/4} \ , \tag{2.2.4}$$

where μ is an energy scale which non-perturbative effect appears, and S is an instanton action. In general, the effective potential of ALPs is given by more than one non-perturbative effect. It is known that in many model f_a and S are related by

$$f_a \sim \frac{M_{\mathrm{pl}}}{S} \ , \tag{2.2.5}$$

where $M_{\rm pl} = 2.4 \times 10^{18}\,\mathrm{GeV}$ is the Planck scale. It is also known that depending on the model, f_a can be significantly lower than Eq. (2.2.5), but f_a never higher than Eq. (2.2.5). Thus Eq. (2.2.5) can be considered as an upper limit. String theory has the potential to provide hundreds of possible values for S. The values of f_a do not change so much between one axion and the other because f_a is inversely proportional to S. However, the value axion mass $m_{a,\rm ALP}$ drastically changes with S, because it depends exponentially. ALPs have wide distributed masses $m_{a,\rm ALP}$ on a log scale.

2.3 Interaction with Photons

Axions interact with photons:

$$\mathcal{L}_{a\gamma\gamma} \equiv -\frac{1}{4}\, g_{a\gamma\gamma}\, a F_{\mu\nu}\tilde{F}_{\mu\nu} = -g_{a\gamma\gamma}\, a\vec{E}\cdot\vec{B}\ , \tag{2.3.1}$$

where $g_{a\gamma\gamma}$ is a coupling constant, $F_{\mu\nu}$ is the field strength of the electromagnetic field and $\tilde{F}_{\mu\nu}$ is its dual. $\vec{E}$ and $\vec{B}$ are electric and magnetic fields, respectively. Although axions also interact with other standard model particles, we dedicate to the two photon coupling. This is because the main subject of this thesis is related to this interaction. Moreover, it is also used as a common strategy for direct axion detection. Laboratory experiments restrict area on parameter plane $(m_a, g_{a\gamma\gamma})$, as we will describe in Sec. 2.5.

Unlike ALPs, the area on the parameter plane $(m_a, g_{a\gamma\gamma})$ which can be occupied by QCD axion is limited due to the proportional relationship between m_a and $g_{a\gamma\gamma}$, Eq. (2.2.1). The width of the QCD axion area comes from the difference of phenomenological models,

$$g_{a\gamma\gamma} = -g_\gamma \frac{\alpha_{\rm EM}}{\pi}\frac{1}{f_a}\ , \tag{2.3.2}$$

where $\alpha_{\rm EM} = 1/137$ is the fine structure constant, and model dependent dimensionless coupling constant g_γ. Kim-Shifman-Vainshtein-Zakharov (**KSVZ**) model [58, 59] $g_\gamma \simeq -0.97$ and Dine-Fischler-Srednicki-Zhitnitsky (**DFSZ**) model [60, 61] $g_\gamma \simeq 0.36$ are frequently referred, but $g_{a\gamma\gamma}$ can take various values for fixed f_a [62].

2.4 Axions as a Dark Matter Candidate

Axion is in the limelight as a dark matter candidate. In this section, we summarize the points which show that axion has adequate features as a dark matter candidate. Please see, *e.g.,* Refs. [63–65] for more details on dark matter in general, not just about axions.

2.4.1 Dark Matter in General

The existence of non-luminous matter began to be pointed out by Zwicky in 1933 [66]. After decades, from the observations of rotation curves, it was suggested that there is mass also in dark places where there are few stars [67,68]. Nowadays, with the addition of various observational data other than the above, we share the awareness for the existence

of such "dark" components, which is called **dark matter**. To reveal the identity of these components is placed as a central problem in modern cosmology.

Observations in the cosmological scales, such as cosmic microwave background (**CMB**) anisotropy and the large scale structure (**LSS**), tell us properties which dark matter should have; that is, dark matter should be pressureless and act nonrelativistic by the time $z \sim 10^7$ [65]. This feature is expressed by the word, **cold**. According to the Planck 2018 analysis of CMB observations, the proportion of cold dark matter in the energy density of the present Universe is $\Omega_{\rm CDM} \sim 0.26$ [69]. In addition, by definition, the dark matter should have feeble interaction with standard model particles such as photons, and its lifetime should be long enough. Please see [63] for details on the conditions which dark matter candidates must meet.

2.4.2 Axions in the Expanding Universe

Let us consider an axion with mass term Eqs. (2.1.4)–(2.1.5). In the early Universe, the axion is constant due to the Hubble friction. In accord with the Universe expands, the Hubble parameter H decreases. When it eventually becomes comparable to the mass of axion $H \sim m_a$, the axion starts to roll down toward the minimum of the potential and begins to oscillate. This coherent oscillation behaves like cold dark matter in the expanding Universe. The axion interaction with other components is so feeble that this oscillation does not dissipate until today and form cold dark matter energy density. This production mechanism of the cold axion is known as the **misalignment mechanism**. In the above, it was implicitly assumed that there is an axion during inflation. If the symmetry breaking occurred after inflation, then there would be other contributions to the relic energy density.

This scenario was firstly pointed out in Refs. [70–72], and the details about axion evolution can be found in, *e.g.,* Refs [44, 45].

2.4.3 Population of Cold QCD Axion

The present density parameter of the cold QCD axion Ω_a is estimated in, *e.g.,* Refs. [45, 46, 73],

$$\Omega_a \equiv \rho_a \frac{8\pi G}{3H_0^2} \ , \tag{2.4.1}$$

where the axion energy density ρ_a is divided by the critical density $\rho_{\rm crit} \equiv 8\pi G/3H_0^2$, and G is gravitational constant, and H_0 is Hubble constant. We quote the result:

$$\Omega_a \sim 0.3\,\Xi \left(\frac{f_a}{10^{12}\,{\rm GeV}} \right)^{\frac{7}{6}} \ , \tag{2.4.2}$$

where Ξ represents uncertainties due to a lack of knowledge about the early Universe. The factor Ξ is affected by whether or not the axion has already existed during inflation, and its value can change approximately by a factor of 10. The condition in Eq. (2.4.2) corresponds to $m_{a,{\rm QCD}} \sim 10^{-5}\,{\rm eV}$ because of the relationship between f_a and $m_{a,{\rm QCD}}$, Eq. (2.2.1). Although there is a possibility that dark matter is composed of several species,

QCD axion, whose mass is heavier than $10^{-3}\,\mathrm{eV}$, cannot be the main component of dark matter. Therefore, if QCD axion is the true identity of dark matter, it is considered that its mass is within the range of $10^{-6}\,\mathrm{eV} \lesssim m_{a,\mathrm{QCD}} \lesssim 10^{-3}\,\mathrm{eV}$, and experiments focusing on this range are also being conducted, see Sec. 2.5.

2.4.4 Decay Rate of Axions

The axion decay to two photons within a lifetime [44, 45],

$$\tau_a = \frac{64\pi}{g_{a\gamma\gamma}^2 m_a^3}\ , \tag{2.4.3}$$

due to the interaction with photons.

In the case of QCD axion, we obtain

$$\tau_{a,\mathrm{QCD}} \simeq \frac{2.79\times 10^{17}}{g_\gamma^2}\,\mathrm{sec}\left(\frac{20\,\mathrm{eV}}{m_{a,\mathrm{QCD}}}\right)^5\ , \tag{2.4.4}$$

by using the relation Eq. (2.2.1). Given the age of the Universe is $t_0 \sim 1.38\times 10^{17}\,\mathrm{sec}$, axion with a mass $m_{a,\mathrm{QCD}} < 20\,\mathrm{eV}$ is stable enough. As mentioned above, there is a stronger upper limit to mass from stellar evolution, see Sec. 2.2.

ALPs have leeway in its mass;

$$\tau_{a,\mathrm{ALP}} \simeq 1.38\times 10^{17}\,\mathrm{sec}\left(\frac{10^{-10}\,\mathrm{GeV}^{-1}}{g_{a\gamma\gamma}}\right)^2\left(\frac{460\,\mathrm{eV}}{m_{a,\mathrm{ALP}}}\right)^3\ , \tag{2.4.5}$$

since coupling $g_{a\gamma\gamma}$ and mass $m_{a,\mathrm{ALP}}$ are not related.

2.4.5 Fuzzy Dark Matter

The ALP whose mass is ultralight $\sim 10^{-22}\,\mathrm{eV}$ is known as a **fuzzy dark matter** [74], and this is an alternative of the cold dark matter scenario. The following is a brief background of why such a substitute model is proposed.

The point is that the property "cold" is drawn from the large scale observations. In other words, it is necessary to carefully test whether the cold dark matter paradigm is also valid in the less than galaxy scale $\lesssim 10\,\mathrm{kpc}$. In fact, it is pointed out that naive simulations assuming cold dark matter can not reproduce some galactic scale observations. This is called the **small scale problem**. Specifically, core-cusp problem, missing satellites problem, and too-big-to-fail problem can be mentioned. All these problems indicate that the amount of structure on a small scale should be suppressed compared to the cold dark matter predictions.

As a solution to the above, the ultralight axion dark matter which make small scale structure "fuzzy" has been proposed. As far as cosmological scale is concerned, the ultralight axion is indistinguishable from the cold dark matter behavior. However, it has a scale below which the structure is erased. Hence, the ultralight axion can successfully compensate for only the shortcomings of the cold dark matter while keeping the success of the cold dark matter intact.

As another approach to the small scale problem, there are simulations which suggest that structure suppression on a small scale can be interpreted as baryonic effects associated with astrophysical processes such as star formations and supernova explosions.

In any case, the small scale problem is a matter of debate and has not been settled and continues to require careful consideration.

2.4.6 Local Dark Matter Density

It is considered that galaxies are surrounded by the so-called **dark matter halo**, which has spread beyond the edge of the visible radius. A standard assumption of the halo is that it goes through gravitational collapse, and now it is in virial equilibrium.

The local dark matter density means an averaged value over a few hundred parsecs around the Sun. Two approaches are often used to measure this local density, namely local measures and global measures. The former are so-called **tracers** and use the kinematics of the stars near the Sun. The latter extrapolates from the rotation curve of the galaxy. In the Reference [75], there is a summary of measurements. We adopt a typical value $0.3\,\mathrm{GeV/cm^3}$ as a dark matter density near the solar system in Sec. 4.5.

Error bars of global measures often small, but they strongly depend on the shape of the dark matter halo. By contrast, local measures have large errors. Putting both observations together, we expect that the shape of the halo would be revealed. Just as the data of the Hipparcos satellite and the Sloan Digital Sky Survey improved local measure's error bars, our understanding of both the Milky Way and the nature of dark matter will be deepened by the Gaia satellite observations.

The upper bound of the local KSVZ axion density with mass range $(2.3 - 3.4)\,\mu\mathrm{eV}$ is given in Ref. [76]; $\rho_{\mathrm{KSVZ}} \lesssim 0.45\,\mathrm{GeV/cm^3}$. There is also an attempt to impose a constraint on the local density of ultralight axion dark matter by using the pulsar timing array, *e.g.,* Ref. [77].

2.5 Search for Axions

Indeed, the detection of axions is challenging due to its feeble interaction, but it might be possible. Over a wide parameter space, including ALPs, various ingenious detection methods towards the first detection of axions have been devised, and some of them are already up and running. In this section, we will take up only the representative examples and explain them briefly. For details on each experiment, please refer to the original papers of each group.

- **Solar Axion**

Due to the axion photon coupling, the Sun is known as a powerful natural axion source. Inside of the Sun, axions are produced from photons in the presence of electromagnetic fields which are produced by the ionized plasma. The energy of the solar axion is comparable to the core temperature of the Sun. The axion flux on the Earth was calculated in Ref. [45]. Solar axion is detected as an X-ray by applying the strong static magnetic field in the laboratory. The CAST experiment at CERN gives the strongest

constraint on the coupling. With an eye to the next generation axion helioscope, IAXO, CAST has improved detectors, and this improvement gives more stringent constraint: $g_{a\gamma\gamma} < 6.6 \times 10^{-11}\,\mathrm{GeV}^{-1}$ for $m_a < 0.02\,\mathrm{eV}$ [78].

• Halo Axion

The most famous strategy is the one which exploits microwave cavities [79–81]. A strong magnetic field is applied in the cavity, and axions are detected as microwaves. This cavity experiment is suitable for a mass range $10^{-7}\,\mathrm{eV} \lesssim m_a \lesssim 10^{-5}\,\mathrm{eV}$. The leading group of this technique is ADMX. Although the mass range is very limited, $(2.81 - 3.31)\,\mu\mathrm{eV}$, this experiment gives the strongest constraint on the coupling: $g_{a\gamma\gamma} \lesssim 3 \times 10^{-16}\,\mathrm{GeV}^{-1}$ [82]. A method has been proposed to target heavier axions than ADMX by using dielectric plates, the so-called MADMAX experiment [83, 84]. By contrast, in the case of lighter mass range, $10^{-9}\,\mathrm{eV} \lesssim m_a \lesssim 10^{-7}\,\mathrm{eV}$, a method which uses LC circuits instead of the cavity has been devised, *e.g.,* the ABRACADABRA experiment [85].

A detailed understanding of the halo is very important for dark matter detection, but it is also true that there are still many uncertainties, as mentioned in Subsec. 2.4.5 and Subsec. 2.4.6. The ADMX's constraints [82] assume both the isothermal model, which is called the standard halo model and the N-body model, which incorporate baryonic physics by using N-body simulation.

• Axion Produced in the Laboratory

There is also an attempt to detect axions which are produced from the laser by applying a magnetic field in the laboratory. Axions, unlike photons, can pass through a wall. Thus, if a magnetic field is applied again over the other side of the wall, and if photons are detected, then it means detection of axions. This observation is a pure experiment which is complete in the laboratory, so it is independent of the physical condition in the Sun. However, these experiments give less constraint for parameter space than the observation of the solar axion. This is due largely to less intensity of the axion flux. This experiment is known as a collective name, **shining light through walls**, *e.g.,* ALPS experiment at DESY: $g_{a\gamma\gamma} < 7 \times 10^{-8}\,\mathrm{GeV}^{-1}$ for $m_a < 5 \times 10^{-4}\,\mathrm{eV}$ [86], and the OSQAR experiment at CERN: $g_{a\gamma\gamma} < 3.5 \times 10^{-8}\,\mathrm{GeV}^{-1}$ for $m_a < 3 \times 10^{-4}\,\mathrm{eV}$ [87]. ALPS is now in preparation for the upgrade experiment [88], and it will go down $g_{a\gamma\gamma} < 2 \times 10^{-11}\,\mathrm{GeV}^{-1}$ for $m_a < 10^{-4}\,\mathrm{eV}$.

• Other Approaches

There are many more ongoing or future experiments which I could not mention. All of the above are experiments using the interaction between axions and photons, as seen in Sec. 2.3, but there are also experiments which use the interaction with fermions. The details of other experiments can be found, *e.g.,* in Refs. [44, 46].

Chapter 3

Conversion Phenomena

In this chapter, we provide an overview of the axion photon conversion. First, in Sec. 3.1, the equations of motion are derived, then we linearize them in Sec. 3.2. Furthermore, we transform them into a commonly used expression in Sec. 3.3. After describing the effects which should be incorporated depending on the situation in Sec. 3.4, we derive the conversion probability analytically in Sec. 3.5. As seen in Sec. 3.6, the conversion also affects the polarization of photons. Finally, we mention some physical applications; that is, the conventional model and the helical model in Sec. 3.7. This thesis deals only with the axion photon conversion, but the graviton photon conversion is known as a similar phenomenon caused by a magnetic field [9, 89, 90].

3.1 Axion Electrodynamics

We consider the following system:

$$S = \int d^4x \left[-\frac{1}{2} \left(\partial_\mu a \, \partial^\mu a + m_a^2 a^2 \right) - \frac{1}{4} F_{\mu\nu} F^{\mu\nu} - \frac{1}{4} \, g_{a\gamma\gamma} \, a F_{\mu\nu} \tilde{F}^{\mu\nu} \right] . \tag{3.1.1}$$

The field strength $F_{\mu\nu}$ of the electromagnetic field A_μ and its dual $\tilde{F}_{\mu\nu}$ are given by

$$F_{\mu\nu} \equiv \partial_\mu A_\nu - \partial_\nu A_\mu \ , \quad \tilde{F}_{\mu\nu} \equiv \frac{1}{2} \epsilon_{\mu\nu\rho\sigma} F^{\rho\sigma} . \tag{3.1.2}$$

From the action Eq. (3.1.1), we can derive the equations of motion for the axion

$$\left(\Box - m_a^2 \right) a = \frac{1}{4} \, g_{a\gamma\gamma} F_{\mu\nu} \tilde{F}^{\mu\nu} \ , \tag{3.1.3}$$

and for the photon

$$\partial_\mu F^{\mu\nu} = -g_{a\gamma\gamma} \, \tilde{F}^{\rho\nu} \partial_\rho a \ . \tag{3.1.4}$$

These equations can be rewritten by using the potential $A_\mu = [-\phi, \vec{A}]$ and the electric and magnetic field,

$$\vec{E} = -\partial_t \vec{A} - \nabla \phi \ , \tag{3.1.5}$$

$$\vec{B} = \nabla \times \vec{A} \ . \tag{3.1.6}$$

We can get the equations for the axion

$$\left(\Box - m_a^2\right) a = g_{a\gamma\gamma}\, \vec{E} \cdot \vec{B} \ , \tag{3.1.7}$$

and for the electromagnetic fields

$$\begin{cases} \Box\, \phi = -g_{a\gamma\gamma}\, \vec{B} \cdot (\nabla a) \ , \\ \Box\, \vec{A} = g_{a\gamma\gamma} \left[(\partial_t\, a)\, \vec{B} + (\nabla\, a) \times \vec{E} \right] \ . \end{cases} \tag{3.1.8}$$

Here, we have chosen the Lorenz gauge:

$$\nabla \cdot \vec{A} + \partial_t\, \phi = 0 \ . \tag{3.1.9}$$

Equations (3.1.7) and (3.1.8) are basic equations of the axion electrodynamics [91]. For the full analysis, we need to resort to numerical calculations. Here, we use the perturbative analysis.

3.2 Perturbative Equations

Let us consider the situation that there is a static and uniform magnetic field in the background. We divide the fields into background and perturbation as follows:

$$\begin{cases} a(z,t) = \ 0 & + \delta a(z,t) \ , \\ \vec{B}(z,t) = \ \vec{B}_0\,(\text{const.}) & + \delta \vec{B}(z,t) \ , \\ \vec{E}(z,t) = \ 0 & + \delta \vec{E}(z,t) \ . \end{cases} \tag{3.2.1}$$

A coordinate basis is introduced so that the propagation is in the direction $\vec{e}_z = [0,0,1]$, one of the rests is parallel to the magnetic field $\vec{e}_\parallel = [1,0,0]$, and the other is $\vec{e}_\perp = [0,1,0]$ (see also Fig. 3.1). That is to say, the background magnetic field is represented as follows:

$$\vec{B}_0 = [B_0, 0, 0] \ . \tag{3.2.2}$$

Since background equations trivially hold, we focus simply on perturbative equations in what follows. Linearizing Eq. (3.1.7) and Eq. (3.1.8), we obtain

$$\begin{cases} \left(\Box - m_a^2\right) \delta a = -g_{a\gamma\gamma}\, B_0 \left(\partial_t\, \delta A_\parallel\right) \ , \\ \Box\, \delta A_\parallel = g_{a\gamma\gamma} B_0\, (\partial_t\, \delta a) \ , \\ \Box\, \delta A_\perp = 0 \ . \end{cases} \tag{3.2.3}$$

Here, we choose the radiation gauge:

$$\delta\phi = 0 \quad \text{and} \quad \nabla \cdot \delta \vec{A} = 0 \ , \tag{3.2.4}$$

since the source term of the equation for the scalar potential vanishes.

From Eq. (3.2.3), we can see that axions and photons have each other's components in the source term. Going one step further, as seen in the next Sec. 3.3, what is called "axion photon conversion" usually denotes the equation, which is reduced to the first-order differential equation [9].

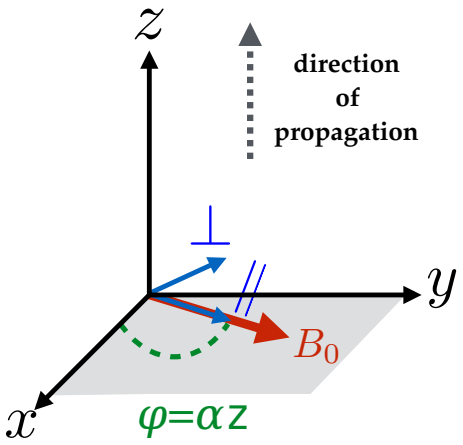

Figure 3.1: The coordinate bases. This figure is quoted from our paper [92]. It is convenient to use the coordinate bases $\vec{e}_{\parallel}$ and $\vec{e}_{\perp}$ according to the direction of the magnetic field when discussing conversion. φ and α are quantities used when considering applications in the physical situation (see Subsec. 3.7.1 and Subsec. 3.7.2). $\vec{e}_x$ and $\vec{e}_y$ are the fixed coordinate system.

3.3 Axion Photon Conversion

If the mass of the axion m_a is sufficiently smaller than the energy of the photons, the energy of the system can be considered to be determined by $\omega \simeq k$. In this case, we can assume axion and photon as follows:

$$\delta a(z,t) \equiv e^{i\omega(z-t)}\,\delta a(z)\ , \tag{3.3.1}$$

$$\delta A_{\parallel}(z,t) \equiv i e^{i\omega(z-t)}\,\delta A_{\parallel}(z)\ . \tag{3.3.2}$$

Here, we have shifted the phase only for the photon in order to make a later equation easier to see. The left hand side of the equation for axion in Eq. (3.2.3) can be rewritten as follows:

$$\begin{aligned}\left(\frac{\partial}{\partial z}\right)^2\left[e^{i\omega(z-t)}\,\delta a(z)\right] &= e^{i\omega(z-t)}\left[\frac{\partial}{\partial z}+i\omega\right]^2\delta a(z)\ ,\\ &\simeq e^{i\omega(z-t)}\left[i2\omega\frac{d}{dz}-\omega^2\right]\delta a(z).\end{aligned} \tag{3.3.3}$$

In the first equal in Eq. (3.3.3), we use following formula:

$$\left(\frac{\partial}{\partial z}\right)^n\left[e^{i\omega z}f(z)\right] = e^{i\omega z}\left[\frac{\partial}{\partial z}+i\omega\right]^n f(z)\ , \tag{3.3.4}$$

where $f(z)$ is an arbitrary function. Considering that $|i2\omega\delta a| \gg |d\,\delta a/dz|$ holds, the formula on the second line is obtained. By applying the same deformation to Eq. (3.2.3), the following equations can be obtained:

$$\begin{cases} i\dfrac{d\delta a}{dz} = \left(\dfrac{m_a^2}{2\omega}\right)\delta a - \dfrac{1}{2}g_{a\gamma\gamma}B_0\delta A_\parallel \ , \\ \\ i\dfrac{d\delta A_\parallel}{dz} = -\dfrac{1}{2}g_{a\gamma\gamma}B_0\delta a \ . \end{cases} \tag{3.3.5}$$

As a result, we obtain the following Schrödinger-like equation,

$$i\frac{d}{dz}\vec{\psi} = \begin{bmatrix} \dfrac{m_a^2}{2\omega} & -\dfrac{1}{2}g_{a\gamma\gamma}B_0 \\ \\ -\dfrac{1}{2}g_{a\gamma\gamma}B_0 & 0 \end{bmatrix}\vec{\psi}, \quad \vec{\psi} \equiv \begin{bmatrix} \delta a(z) \\ \delta A_\parallel(z) \end{bmatrix}, \tag{3.3.6}$$

and this equation is the fundamental equation of **axion photon conversion**. The matrix in the right hand side is called the **mixing matrix**. The mass term of axion is denoted by

$$\Delta_a \equiv \frac{m_a^2}{2\omega} \ , \tag{3.3.7}$$

and the mixing term is denoted by

$$\Delta_{a\gamma} \equiv -\frac{1}{2}g_{a\gamma\gamma}B_0 \ . \tag{3.3.8}$$

As a side note, if we assumed

$$\delta A_\parallel(z,t) = e^{i\omega(z-t)}\,\delta A_\parallel(z) \ ,$$

in Eq. (3.3.2), then the mixing matrix would be a Hermitian matrix.

3.4 Effective Mass of Photon

So far, we assumed that only axions have a very small mass, but photons can also have an effective mass by some effects. In this section, we consider them.

The first effect is the plasma effect. The dispersion relation of the electromagnetic waves propagating in the plasma is corrected as follows:

$$\omega^2 = k^2 + \omega_p^2, \quad \omega_p^2 \equiv 4\pi\alpha_{\rm EM}\frac{n_e}{m_e} \ , \tag{3.4.1}$$

where $\alpha_{\rm EM}$ is the fine structure constant, and n_e is the electron density, and m_e is the electron mass. We choose the natural Lorentz-Heaviside units. If one assumes that all the hydrogen atoms existing in the Universe are ionized by reionization and if one chooses electron density in outer space, $n_e \simeq 10^{-7}\,{\rm cm}^{-3}$, then the effective mass is approximately

$$\omega_p = 1.17\times10^{-14}\,{\rm eV}\Big(\frac{n_e}{10^{-7}\,{\rm cm}^{-3}}\Big) \ . \tag{3.4.2}$$

The second effect is the QED effect. The corrections in the limit of $\omega \sim k \ll m_e$ is given by **Euler-Heisenberg lagrangian**:

$$\mathcal{L}_{\rm EH} = \frac{\alpha_{\rm EM}^2}{90 m_e^4}\left[(F_{\mu\nu}F^{\mu\nu})^2 + \frac{7}{4}\left(\tilde{F}_{\mu\nu}F^{\mu\nu}\right)^2\right] . \tag{3.4.3}$$

Incorporating the above two effects, the left hand side formula corresponding to Eq. (3.2.3) is corrected as follows:

$$(\Box + 7\varrho_{\rm QED}\,\omega^2 B_0^2 - \omega_p^2)\delta A_\parallel = g_{a\gamma\gamma}B_0\,(\partial_t\,\delta a) , \tag{3.4.4}$$

$$(\Box + 4\varrho_{\rm QED}\,\omega^2 B_0^2 - \omega_p^2)\delta A_\perp = 0 . \tag{3.4.5}$$

Thus, we can define following quantities:

$$\Delta_{\rm plasma} \equiv \frac{\omega_p^2}{2\omega} , \tag{3.4.6}$$

$$\Delta_{\rm QED}^{\parallel} \equiv -\frac{7}{2}\omega\varrho_{\rm QED}B_0^2 , \tag{3.4.7}$$

$$\Delta_{\rm QED}^{\perp} \equiv -2\omega\varrho_{\rm QED}B_0^2 , \tag{3.4.8}$$

as components of the mixing matrix which represents the effective mass of photons. Here, we define

$$\varrho_{\rm QED}B_0^2 \equiv \frac{\alpha_{\rm EM}}{45\pi}\left(\frac{e}{m_e^2}\right)^2 B_0^2 = \frac{\alpha_{\rm EM}}{45\pi}\left(\frac{B_0}{B_{\rm cr}}\right)^2 , \tag{3.4.9}$$

with

$$B_{\rm cr} \equiv \frac{m_e^2}{e} = 4.42\times 10^{13}\,{\rm G} . \tag{3.4.10}$$

3.5 Conversion Probability

Let us evaluate a conversion probability by solving the equation,

$$i\frac{d}{dz}\vec{\psi} = \mathbf{M}_\parallel\vec{\psi}, \quad \mathbf{M}_\parallel \equiv \begin{bmatrix}\Delta_a & \Delta_{a\gamma}\\ \Delta_{a\gamma} & \Delta_\parallel\end{bmatrix} , \tag{3.5.1}$$

where $\Delta_\parallel$ is the mass term of photon, *i.e.,* $\Delta_{\rm plasma}$ and/or $\Delta_{\rm QED}^{\parallel}$. Since the mixing matrix $\mathbf{M}_\parallel$ is a symmetric matrix, it can be diagonalized by using an orthogonal matrix $\mathbf{O}$,

$$\mathbf{O^{-1}M}_\parallel\mathbf{O} = \begin{bmatrix}\lambda_+ & 0\\ 0 & \lambda_-\end{bmatrix} , \quad \mathbf{O} \equiv \begin{bmatrix}\cos\theta & -\sin\theta\\ \sin\theta & \cos\theta\end{bmatrix} , \tag{3.5.2}$$

where θ is called the **mixing angle**, and $\lambda_\pm$ are eigenvalues,

$$\lambda_\pm \equiv \frac{1}{2}\left[(\Delta_a + \Delta_\parallel) \pm \sqrt{(\Delta_a - \Delta_\parallel)^2 + (2\Delta_{a\gamma})^2}\right] . \tag{3.5.3}$$

Therefore, we can solve Eq. (3.5.1) as follows:

$$\psi_i(z) = \sum_{j=1}^{2} \mathbf{O}_{ij} \Big[\mathbf{O}^{-1}\vec{\psi}(0)\Big]_j e^{-\lambda_j z} \ , \tag{3.5.4}$$

where $\lambda_1 \equiv \lambda_+$ and $\lambda_2 \equiv \lambda_-$; that is,

$$\delta a(z) = \big[\cos^2\theta e^{-i\lambda_+ z} + \sin^2\theta e^{-i\lambda_- z}\big]\delta a(0) + \cos\theta\sin\theta\big[e^{-i\lambda_+ z} - e^{-i\lambda_- z}\big]\delta A_\parallel(0) \ , \tag{3.5.5}$$

$$\delta A_\parallel(z) = \cos\theta\sin\theta\big[e^{-i\lambda_+ z} - e^{-i\lambda_- z}\big]\delta a(0) + \big[\sin^2\theta e^{-i\lambda_+ z} + \cos^2\theta e^{-i\lambda_- z}\big]\delta A_\parallel(0) \ . \tag{3.5.6}$$

For example, when we choose $\delta a(0) = 0$ and $\delta A_\parallel(0) = 1$, the conversion probability of the photon into the axion after traveling a distance z is given as follows:

$$P_0(z) \equiv (\sin 2\theta)^2 \sin^2\left[\frac{\sqrt{(\Delta_a - \Delta_\parallel)^2 + (2\Delta_{a\gamma})^2}}{2} z\right] . \tag{3.5.7}$$

We refer to

$$\Delta_{\rm osc} \equiv \lambda_+ - \lambda_- = \sqrt{(\Delta_a - \Delta_\parallel)^2 + (2\Delta_{a\gamma})^2} \ , \tag{3.5.8}$$

as the **oscillation length**. If one realizes the following relation,

$$\sin 2\theta = \frac{2\Delta_{a\gamma}}{\Delta_{\rm osc}} \ , \tag{3.5.9}$$

then we can rewrite Eq. (3.5.7) as follows:

$$P_0(z) = (\Delta_{a\gamma} z)^2 \frac{\sin^2\left(\dfrac{\Delta_{\rm osc}}{2} z\right)}{\left(\dfrac{\Delta_{\rm osc}}{2} z\right)^2} \ . \tag{3.5.10}$$

The axion photon conversion is the most effective when the following condition is satisfied:

$$\Delta_{a\gamma} \gg |\Delta_a - \Delta_\parallel| \ , \tan 2\theta_{\rm s} = \frac{2\Delta_{a\gamma}}{\Delta_a - \Delta_\parallel} \gg 1 \ . \tag{3.5.11}$$

In this case, $\theta_{\rm s} \sim \pi/4$ and $\Delta_{\rm osc,s} \simeq 2\Delta_{a\gamma}$. Here, the subscript "s" is added to clearly indicate that this is the case for strong coupling. When $\Delta_{\rm osc} \ll 1$ holds, Eq. (3.5.10) can be further simplified:

$$P_0(z) \simeq (\Delta_{a\gamma}\, z)^2 \ . \tag{3.5.12}$$

3.6 Effects on the Polarization of Photons

Since only one of the photon's two components can mix with the axion, the axion photon conversion can affect the polarization of photons. The photon polarization is described in the context of **Stokes parameters** (I, Q, U, V),

$$\begin{cases} I(z) & \equiv \delta A_\parallel \delta A_\parallel^* + \delta A_\perp \delta A_\perp^* \ , \\ Q(z) & \equiv \delta A_\parallel \delta A_\parallel^* - \delta A_\perp \delta A_\perp^* \ , \\ U(z) & \equiv \delta A_\parallel \delta A_\perp^* + \delta A_\perp \delta A_\parallel^* \ , \\ V(z) & \equiv i \left[\ \delta A_\parallel \delta A_\perp^* - \delta A_\perp \delta A_\parallel^* \right] \ . \end{cases} \tag{3.6.1}$$

They satisfy a following equation.

$$I^2(z) \ = \ Q^2(z) + U^2(z) + V^2(z) \ . \tag{3.6.2}$$

Note that $I(z)$ and $V(z)$ are invariant under the coordinate transformation, but $Q(z)$ and $U(z)$ depend on the coordinate system. Using the intensity of the photon $I(z)$, we can define the degree of circular polarization

$$\Pi_C \ = \ \frac{|V(z)|}{I(z)} \ , \tag{3.6.3}$$

and the degree of linear polarization,

$$\Pi_L \ = \ \frac{\sqrt{Q^2(z) + U^2(z)}}{I(z)} \ . \tag{3.6.4}$$

Since $\delta A_\perp$ which do not participate in the conversion must be included in the calculation of Stokes parameters, we redefine the mixing matrix $\mathbf{M}$ as follows:

$$i \frac{d}{dz} \vec{\Psi} = \mathbf{M} \vec{\Psi} \ , \quad \mathbf{M} \equiv \begin{bmatrix} \Delta_a & \Delta_{a\gamma} & 0 \\ \Delta_{a\gamma} & \Delta_\parallel & 0 \\ 0 & 0 & \Delta_\perp \end{bmatrix} \ , \quad \vec{\Psi} \equiv \begin{bmatrix} \delta a(z) \\ \delta A_\parallel(z) \\ \delta A_\perp(z) \end{bmatrix} \tag{3.6.5}$$

Stokes parameters can be calculated by using Eq. (3.5.5) and Eq. (3.5.6), but they have a simpler form in the case of $\Delta_\parallel = \Delta_\perp = \Delta_{\rm plasma}$, because the polarization depends only on $(\Delta_a - \Delta_{\rm plasma})$. The Stokes parameters do not change when we redefine the field as $\Psi_i e^{-i\Delta_{\rm plasma} z}$. While the mixing matrix is transformed as

$$\mathbf{M} = \begin{bmatrix} \Delta_a - \Delta_{\rm plasma} & \Delta_{a\gamma} & 0 \\ \Delta_{a\gamma} & 0 & 0 \\ 0 & 0 & 0 \end{bmatrix} \ . \tag{3.6.6}$$

Thus, we can consider only the case $\Delta_{\rm plasma} = 0$ without loss of generality. The result in the case $\Delta_{\rm plasma} \neq 0$ can be obtained by replacing Δ_a with $(\Delta_a - \Delta_{\rm plasma})$. Under the assumption $\Delta_\parallel = \Delta_\perp = \Delta_{\rm plasma}$ and an initial condition: $\delta a(0) = 0$ and $V_0 = 0$, we can evaluate polarizations as follows:

$$I(z) = I_0 - (I_0 + Q_0) \left(\frac{\Delta_M}{\Delta_{osc}} \right)^2 \left[1 - \cos\left(\Delta_{osc} z \right) \right] \ , \tag{3.6.7}$$

$$Q(z) = Q_0 - (I_0 + Q_0)\left(\frac{\Delta_M}{\Delta_{osc}}\right)^2 \left[1 - \cos\left(\Delta_{osc} z\right)\right] \ , \tag{3.6.8}$$

$$U(z) = \frac{U_0 \Delta_M^2}{\Delta_{osc}} \left[\frac{\cos(\lambda_+ z)}{\lambda_+} - \frac{\cos(\lambda_- z)}{\lambda_-}\right] \ , \tag{3.6.9}$$

$$\Pi_C(z) \ = \ \left| \frac{U_0(\Delta_M^2/\Delta_{osc})}{I_0 - (I_0 + Q_0)(\Delta_M/\Delta_{osc})^2 \left[1 - \cos(\Delta_{osc} z)\right]} \left[\frac{\sin(\lambda_+ z)}{\lambda_+} - \frac{\sin(\lambda_- z)}{\lambda_-}\right] \right| \ , \tag{3.6.10}$$

where I_0, Q_0, U_0 represent the initial Stokes parameters.

3.7 Application for Cosmological Magnetic Field

As we have seen in Chap. 1, the Universe is magnetized. There are various studies on the conversion caused by the magnetic field existing in the Universe [16–42]. In this section, we would like to review two cases, namely the conventional model and the helical model.

3.7.1 Conventional Model

In this model, we divide the line of sight into domains which have equal lengths s. Within each domain, the direction of the magnetic field is constant, but between domains, its direction randomly changes. Photons which are emitted from a source in the cosmological distance travel through these domains to us on the Earth. The strength of the magnetic field is assumed to be the same in all domains. We refer to this scenario as the **conventional model** in this thesis. In what follows, we give the total conversion probability after passing N-domains, according to Ref. [19]. We also evaluate the variance of polarization in the same way Ref. [92].

The length of one domain is given by s, so the conversion probability within a single domain is obtained from Eq. (3.5.10):

$$P_0(s) = (\Delta_{a\gamma} s)^2 \frac{\sin^2\left(\dfrac{\Delta_{\rm osc}}{2} s\right)}{\left(\dfrac{\Delta_{\rm osc}}{2} s\right)^2} \ . \tag{3.7.1}$$

Any coordinate system can be used as long as the invariant quantity is concerned, such as I, Π_C and Π_L. We define the n-th domain as $z_{n-1} < z \leqq z_n$. The angle between $\vec{B}_0$ in the n-th domain and the fixed x-axis is denoted as $0 \leqq \varphi_n \leqq 2\pi$, and we set initial condition $\varphi_0 = 0$ (see Fig. 3.1). Now, we evaluate the total conversion probability after passing N-domains. The relationship between the $(n-1)$-th domain and n-th domain is

given by

$$
\begin{aligned}
a^n(z_n) &= \left[\cos^2\theta\, e^{-i\lambda_+ s} + \sin^2\theta\, e^{-i\lambda_- s}\right] a(z_{n-1}) \\
&\quad + \cos\theta\sin\theta\left[e^{-i\lambda_+ s} - e^{-i\lambda_- s}\right]\left[\cos\gamma_n\, A_\parallel^{n-1}(z_{n-1}) + \sin\gamma_n\, A_\perp^{n-1}(z_{n-1})\right] \ , \qquad (3.7.2)\\
A_\parallel^n(z_n) &= \cos\theta\sin\theta\left[e^{-i\lambda_+ s} - e^{-i\lambda_- s}\right] a(z_{n-1}) \\
&\quad + \left[\sin^2\theta\, e^{-i\lambda_+ s} + \cos^2\theta\, e^{-i\lambda_- s}\right]\left[\cos\gamma_n\, A_\parallel^{n-1}(z_{n-1}) + \sin\gamma_n\, A_\perp^{n-1}(z_{n-1})\right] \ , \qquad (3.7.3)\\
A_\perp^n(z_n) &= -\sin\gamma_n\, A_\parallel^{n-1}(z_{n-1}) + \cos\gamma_n\, A_\perp^{n-1}(z_{n-1}) \ , \qquad (3.7.4)
\end{aligned}
$$

where $\gamma_n \equiv \varphi_n - \varphi_{n-1}$. The intensity of the photon and the axion at the end of the n-th domain is represented by quantities of the $(n-1)$-th domain

$$
\begin{aligned}
I(z_n) &= P_0|a(z_{n-1})|^2 + (1 - P_0\cos^2\gamma_n)|A_\parallel^{n-1}(z_{n-1})|^2 \\
&\quad + (1 - P_0\sin^2\gamma_n)|A_\perp^{n-1}(z_{n-1})|^2 + \cdots \ , \qquad (3.7.5)
\end{aligned}
$$

$$
\begin{aligned}
I_a(z_n) &= (1 - P_0)|a(z_{n-1})|^2 + \cos^2\gamma_n P_0|A_\parallel^{n-1}(z_{n-1})|^2 \\
&\quad + \sin^2\gamma_n P_0|A_\perp^{n-1}(z_{n-1})|^2 + \cdots \ , \qquad (3.7.6)
\end{aligned}
$$

where the dots represent terms which are proportional to $\cos\gamma_n$, $\sin\gamma_n$, or $\cos\gamma_n\sin\gamma_n$. We assume that the angles γ_n are randomly chosen. Because of the randomness, $\cos^2\gamma_n$ and $\sin^2\gamma_n$ can be replaced by their average value $1/2$, and the other terms are averaged to zero. We obtain the recursion relation,

$$
\begin{bmatrix} I(z_n) \\ \\ I_a(z_n) \end{bmatrix} \equiv \mathbf{W} \begin{bmatrix} I(z_{n-1}) \\ \\ I_a(z_{n-1}) \end{bmatrix} \ , \quad \mathbf{W} \equiv \begin{bmatrix} 1 - P_0/2 & P_0 \\ \\ P_0/2 & 1 - P_0 \end{bmatrix} \ . \qquad (3.7.7)
$$

We can evaluate the eigenvalues $w_\pm$ of the matrix $\mathbf{W}$,

$$
w_\pm \equiv \frac{1}{2}\left[\left(2 - \frac{3}{2}P_0\right) \pm \frac{3}{2}P_0\right] \ . \qquad (3.7.8)
$$

From the recursion relation Eq. (3.7.7), we obtain the following relation:

$$
\begin{bmatrix} I(z_n) \\ \\ I_a(z_n) \end{bmatrix} = \frac{1}{3}\begin{bmatrix} 2 + (1 - 3P_0/2)^n & 2 - 2\,(1 - 3P_0/2)^n \\ \\ 1 - (1 - 3P_0/2)^n & 1 + 2\,(1 - 3P_0/2)^n \end{bmatrix} \begin{bmatrix} I(z_0) \\ \\ I_a(z_0) \end{bmatrix} \ . \qquad (3.7.9)
$$

Noticing that $n = z/s$ gives a number of domains and using the relation $e^x = \lim_{n\to\infty}(1 + x/n)^n$, a part of the components of the matrix in Eq. (3.7.9) can be rewritten as follows:

$$
\left(1 - \frac{3}{2}P_0\right)^n = \left(1 + \frac{-3P_0/2}{z/s}z/s\right)^n = \left(1 + \frac{-3P_0/2s}{n}z\right)^n \xrightarrow[n\to\infty]{} \exp\left(-\frac{3P_0}{2s}z\right) .
$$

In the end, we obtain the following expressions

$$\begin{aligned} I(z) &= I(z_0) - P_{\gamma\to a}[I(z_0) - 2I_a(z_0)] \,, \\ I_a(z) &= I_a(z_0) + P_{\gamma\to a}[I(z_0) - 2I_a(z_0)] \,, \end{aligned} \tag{3.7.10}$$

with

$$P_{\gamma\to a} \equiv \frac{1}{3}\left[1 - \exp\left(-\frac{3P_0}{2s}z\right)\right] \,. \tag{3.7.11}$$

In the limit $n = z/s \to \infty$, the conversion probability saturates so that on average one third of all photons converts to axions.

We can obtain the same limit for other quantities [92]. To this end, we introduce a density matrix and Stokes parameters (I, Q, U, V)

$$\begin{aligned} \boldsymbol{\rho}(z) &\equiv \begin{bmatrix} \delta a(z) \\ \delta A_\parallel(z) \\ \delta A_\perp(z) \end{bmatrix} \otimes \left[\delta a^*(z)\ \delta A_\parallel^*(z)\ \delta A_\perp^*(z)\right] \\ &= \begin{bmatrix} I_a(z) & \frac{K(z) - iL(z)}{2} & \frac{M(z) - iN(z)}{2} \\ \frac{K(z) + iL(z)}{2} & \frac{I(z) + Q(z)}{2} & \frac{U(z) - iV(z)}{2} \\ \frac{M(z) + iN(z)}{2} & \frac{U(z) + iV(z)}{2} & \frac{I(z) - Q(z)}{2} \end{bmatrix} \,, \end{aligned} \tag{3.7.12}$$

where we defined $2\,\delta a\,\delta A_\parallel^* = K - iL$ and $2\,\delta a\,\delta A_\perp^* = M - iN$. Repeating the same analysis with polarization degrees of freedom, we obtained the asymptotic values,

$$I_a = \frac{1}{3}\ , I = \frac{2}{3}\ , Q = U = V = K = L = M = N = 0\ : \tag{3.7.13}$$

that is, the polarization vanishes on average. Now, we evaluate the variance of polarizations. It is useful to notice that the density matrix obeys following equation:

$$i\frac{d\boldsymbol{\rho}(z)}{dz} \;=\; [\mathbf{M}, \boldsymbol{\rho}(z)] \,.$$

If we define the transfer function $\mathbf{T}(z, z_0)$ with initial condition $\mathbf{T}(z_0, z_0) = 1$, then we can formally solve the dynamics:

$$\boldsymbol{\rho}(z) \;=\; \mathbf{T}(z, z_0)\,\boldsymbol{\rho}(z_0)\,\mathbf{T}^\dagger(z, z_0) \,. \tag{3.7.14}$$

$\boldsymbol{\rho}^2(z)$ also obeys the same equation,

$$\boldsymbol{\rho}^2(z) \;=\; \mathbf{T}(z, z_0)\,\boldsymbol{\rho}^2(z_0)\,\mathbf{T}^\dagger(z, z_0) \,. \tag{3.7.15}$$

This implies that the corresponding components of $\boldsymbol{\rho}^2(z)$ have the same limit values as those in Eq. (3.7.13). From the explicit calculation, we obtain,

$$\boldsymbol{\rho}^2(z) = \begin{bmatrix} I_a^2 + \frac{K^2+L^2+M^2+N^2}{4} & \text{cross terms} & \text{cross terms} \\ \text{cross terms} & \frac{K^2+L^2+(I+Q)^2+U^2+V^2}{4} & \text{cross terms} \\ \text{cross terms} & \text{cross terms} & \frac{M^2+N^2+(I-Q)^2+U^2+V^2}{4} \end{bmatrix} \,, \tag{3.7.16}$$

and the asymptotic values

$$I_a^2 + \frac{K^2 + L^2 + M^2 + N^2}{4} = \frac{1}{3} \,, \tag{3.7.17}$$

$$\frac{I^2 + Q^2 + U^2 + V^2}{2} + \frac{K^2 + L^2 + M^2 + N^2}{4} = \frac{2}{3} \,, \tag{3.7.18}$$

$$K^2 + L^2 - M^2 - N^2 = 0 \,, \tag{3.7.19}$$

$$\text{cross terms} = 0 \,, \tag{3.7.20}$$

where we ignored the average of the cross terms such as IQ because of the statistical independence of these variables. Assuming equi-partition for $I_a^2, Q^2, U^2, V^2, K^2, L^2, M^2, N^2$ and taking into account the relation $I^2 = Q^2 + U^2 + V^2$, we can conclude

$$I_a^2 = \frac{1}{6} \,, I^2 = \frac{1}{2} \,, Q^2 = \frac{1}{6} \,, U^2 = \frac{1}{6} \,, V^2 = \frac{1}{6} \,. \tag{3.7.21}$$

These results are confirmed by the numerical calculation as shown in Fig. 3.2. Using the value in Eq. (3.7.21), we can analytically calculate the degree of the circular polarization

$$\Pi_C \;=\; \sqrt{\frac{V^2}{I^2}} = 0.577 \,, \tag{3.7.22}$$

and the degree of the linear polarization

$$\Pi_L \;=\; \sqrt{\frac{Q^2 + U^2}{I^2}} = 0.816 \,. \tag{3.7.23}$$

The latter shows a good agreement with the numerical result in Ref. [34].

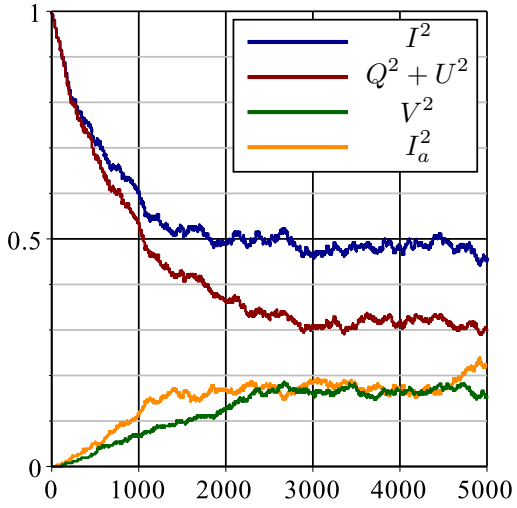

Figure 3.2: This figure is quoted from our paper [92]. The evolution of mean-square values of the polarization and the intensity throughout 5000 domains for the conventional model. We took the average of 100 times trial. Since the average values of the polarizations are zero, Q^2, U^2, and V^2 are the variances. We set $\Delta_a = 1.5 \times 10^{-2}$ Mpc^{-1}, $\Delta_M = 3.0 \times 10^{-2}$ Mpc^{-1}.

3.7.2 Helical Model

Primordial magnetogenesis models, *e.g.,* inflation, predict coherent magnetic fields over the cosmological distance and suggest that it can have a magnetic helicity $\vec{H}$ [1, 2],

$$\vec{H} \equiv \int d^3x\, \vec{A} \cdot \left(\nabla \times \vec{A} \right) . \tag{3.7.24}$$

For example, Refs. [92–95] can be mentioned as studies considering the axion photon conversion under this configuration.

• Helical Single Domain Model

We consider the situation where the direction of the magnetic field changes within a single domain in terms of the fixed $x - y$ coordinate system:

$$\vec{B}_{\rm helical} \equiv B_0 \, \cos(\alpha z) \vec{e}_x + B_0 \, \sin(\alpha z) \vec{e}_y \, . \tag{3.7.25}$$

In this case, the linearized equations of motion corresponding to Eq. (3.2.3) is as follows:

$$\begin{cases} \left(\Box - m_a^2 \right) \delta a = -g_{a\gamma\gamma} \, B_0 \left[(\partial_t \, \delta A_x) \cos(\alpha z) + (\partial_t \, \delta A_y) \sin(\alpha z) \right] , \\ \Box \, \delta A_x = g_{a\gamma\gamma} B_0 \, (\partial_t \, \delta a) \cos(\alpha \, z) \, , \\ \Box \, \delta A_y = g_{a\gamma\gamma} B_0 \, (\partial_t \, \delta a) \sin(\alpha \, z) \, . \end{cases} \tag{3.7.26}$$

Just like Sec. 3.3, we can reduce the first-order differential equations:

$$i \frac{d}{dz} \begin{bmatrix} \delta a(z) \\ \delta A_x(z) \\ \delta A_y(z) \end{bmatrix} = \begin{bmatrix} \Delta_a & \Delta_{a\gamma} \cos(\alpha z) & \Delta_{a\gamma} \sin(\alpha z) \\ \Delta_{a\gamma} \cos(\alpha z) & \Delta_{xx} & \Delta_{xy} \\ \Delta_{a\gamma} \sin(\alpha z) & \Delta_{yx} & \Delta_{yy} \end{bmatrix} \begin{bmatrix} \delta a(z) \\ \delta A_x(z) \\ \delta A_y(z) \end{bmatrix} , \tag{3.7.27}$$

with

$$\begin{aligned} \Delta_{xx} &= \Delta_\parallel \cos^2(\alpha z) + \Delta_\perp \sin^2(\alpha z) \, , \\ \Delta_{xy} &= \Delta_{yx} = (\Delta_\parallel - \Delta_\perp) \cos(\alpha z) \sin(\alpha z) \, , \\ \Delta_{yy} &= \Delta_\parallel \sin^2(\alpha z) + \Delta_\perp \cos^2(\alpha z) \, . \end{aligned}$$

Here, $\Delta_\parallel$ and $\Delta_\perp$ represent effective photon mass as we have already seen in the Sec. 3.4. The correction to $\Delta_{\rm QED}$ due to the magnetic field becoming z dependent can be ignored.

We perform a unitary transformation $\mathbf{U}$,

$$\begin{bmatrix} \delta a(z) \\ \delta A_\parallel(z) \\ \delta A_\perp(z) \end{bmatrix} = \mathbf{U} \begin{bmatrix} \delta a(z) \\ \delta A_x(z) \\ \delta A_y(z) \end{bmatrix} , \quad \mathbf{U} \equiv \begin{bmatrix} 1 & 0 & 0 \\ 0 & \cos(\alpha z) & \sin(\alpha z) \\ 0 & -\sin(\alpha z) & \cos(\alpha z) \end{bmatrix} ,$$

and change the coordinate basis from the $x - y$ coordinate to the $\parallel - \perp$ coordinate.

$$i \frac{d}{dz} \vec{\Psi} = \mathbf{M}_{\rm helical} \vec{\Psi} \, , \quad \mathbf{M}_{\rm helical} \equiv \begin{bmatrix} \Delta_a & \Delta_{a\gamma} & 0 \\ \Delta_{a\gamma} & \Delta_\parallel & i\alpha \\ 0 & -i\alpha & \Delta_\perp \end{bmatrix} , \quad \vec{\Psi} \equiv \begin{bmatrix} \delta a(z) \\ \delta A_\parallel(z) \\ \delta A_\perp(z) \end{bmatrix} . \tag{3.7.28}$$

• Configuration Dependence of Polarization

As is the case for the conventional model in Subsec. 3.7.1, we picture the situation that linearly polarized photons propagate through an area which consist of connecting a series of equal distance single domains. References [95] and [92] share the feature of the helical magnetic field within a single domain. We refer to this situation as the **Helical model** in this thesis. However, the way to connect areas is different, respectively. In the following, we discuss the magnetic field configuration dependence of the effect of the axion photon conversion on polarization, mainly along Ref. [92]. Please see references for details on the differences between the two models, Refs. [95] and [92].

We set the domain size $s = 1\,\mathrm{Mpc}$ and take α as a random variable uniformly distributed within a range. The range of α determines the coherent length of the cosmological magnetic field. α changes randomly from domains to domains, but the strength of magnetic fields is fixed for simplicity. As a formality, we can obtain the transfer function $\mathbf{T}(z, z_0)$ in the same way as in the conventional model Subsec. 3.7.1. However, in the case of the helical magnetic fields, the matrix $\mathbf{O}_{\mathrm{helical}}$ which diagonalizes the mixing matrix $\mathbf{M}_{\mathrm{helical}}$ has a complicated dependence on the parameters, so we have to resort to numerical calculations.

We solve Eq. (3.7.28) numerically in order to examine the evolution of the mean-square values of the polarization and intensity. In Fig. 3.3, we plotted the evolution of the mean-square values for relevant quantities for the range $|\alpha| \leq \pi\,\mathrm{Mpc}^{-1}$. The behavior of mean-square values is quite similar to those in the conventional model. In this case, since the helical configuration changes significantly, the cancellation occurs, and the mean-square values converge to the asymptotic values in the same way as the conventional model. On the other hand, if we make the range for α small, then the behavior peculiar to the helical model appears. In Fig. 3.4, we plotted the evolution of the mean-square values for relevant quantities for the range $|\alpha| \leq \pi/36\,\mathrm{Mpc}^{-1}$. In the early stage of evolution, each value behaves as a damped oscillation, and the speed of the convergence to the asymptotic values becomes slow. At first, since the change of the configuration is small, the cancellation rarely occurs, and the mean-square values oscillate in the same way as the case $\alpha = 0$. However, after traversing many domains, each mean-square values end up with the asymptotic value. Thus, the converging behavior itself is universal. The narrower the range of α, the slower the speed of the convergence is. In short, the small range for α makes the effective coherence length long and creates a similar situation in which the magnetic field is fixed. However, since the magnetic field is not completely constant, mean-square values converge before long.

In Ref. [92], attempts are also being made to constrain parameters on the condition that it does not conflict with the current observation by using the transient behavior.

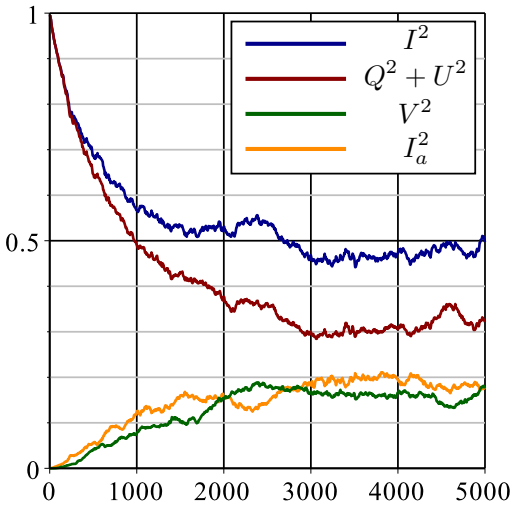

Figure 3.3: This figure is quoted from our paper [92]. The evolution of mean-square values of the polarization and the intensity throughout 5000 domains for the helical domain model with $|\alpha| \leq \pi\,\mathrm{Mpc}^{-1}$. We took the average of 100 times trial. Since the average values of the polarization are zero, Q^2, U^2, and V^2 are the variances. We set $\Delta_a = 1.5 \times 10^{-2}$ Mpc^{-1}, $\Delta_M = 3.0 \times 10^{-2}$ Mpc^{-1}.

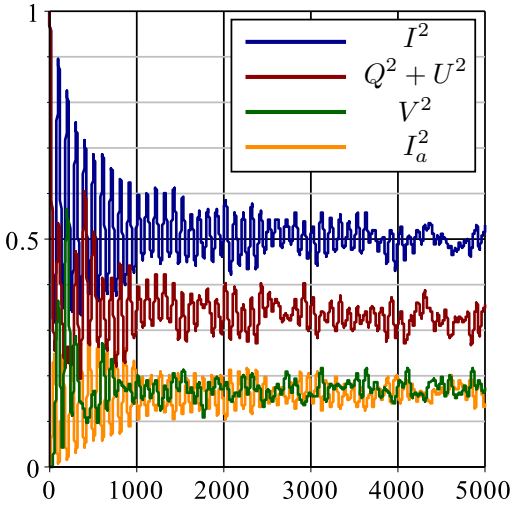

Figure 3.4: This figure is quoted from our paper [92]. The evolution of mean-square values of the polarization and the intensity throughout 5000 domains for the helical domain model with $|\alpha| \leq \pi/36\,\mathrm{Mpc}^{-1}$. We took the average of 100 times trial. Since the average values of the polarization are zero, Q^2, U^2, and V^2 are the variances. In this plot, we used the parameters $\Delta_a = 1.5{\times}10^{-2}\,\mathrm{Mpc}^{-1}$, $\Delta_M = 3.0{\times}10^{-2}\,\mathrm{Mpc}^{-1}$.

Chapter 4

Axion Dark Matter Photon Conversion

The main topic is given in this chapter. Assuming that axion is the identity of dark matter, we study the conversion phenomena [43]. The starting point is the same as before, Sec. 3.1. We repeat the basic equations below. The equation of motion for the axion is as follows:

$$\left(\Box - m_a^2\right) a = g_{a\gamma\gamma}\, \vec{E} \cdot \vec{B} \ , \tag{3.1.7}$$

and for electromagnetic fields,

$$\begin{cases} \Box\, \phi = -g_{a\gamma\gamma}\, \vec{B} \cdot (\nabla a) \ , \\ \Box\, \vec{A} = g_{a\gamma\gamma} \left[(\partial_t\, a)\, \vec{B} + (\nabla\, a) \times \vec{E} \right] \ , \end{cases} \tag{3.1.8}$$

with the Lorenz gauge:

$$\nabla \cdot \vec{A} + \partial_t\, \phi = 0 \ . \tag{3.1.9}$$

We divide the fields into the background and the perturbation as follows:

$$\begin{cases} a(z,t) = \ a_0(t) & + \delta a(z,t) \ , \\ \vec{B}(z,t) = \ \vec{B}_0\,(\text{const.}) & + \delta \vec{B}(z,t) \ , \\ \vec{E}(z,t) = \ \vec{E}_0(t) & + \delta \vec{E}(z,t) \ . \end{cases} \tag{4.0.1}$$

Unlike the situation where there is only a static magnetic field, we need to solve the equations (3.1.7) and (3.1.8) not only for perturbative quantities (Sec. 4.2) but also for background quantities (Sec. 4.1).

In both Sec. 4.3 and Sec. 4.4, we use the knowledge about the Mathieu equation without explanation. Instead, we summarize minimum knowledge about the Mathieu equation in Appx. A. In Sec. 4.5, we also touch on physical application.

4.1 Background Equations

We assume that both a static magnetic field,

$$\vec{B}_0 = [B_0, 0, 0] \ , \tag{4.1.1}$$

and a coherent oscillating axion $a_0(t)$ exist in the background. The coordinate bases are the same as for Sec. 3.2: the propagation direction $\vec{e}_z = [0, 0, 1]$, the direction parallel to the magnetic field $\vec{e}_\parallel = [1, 0, 0]$ and the direction normal to the magnetic field $\vec{e}_\perp = [0, 1, 0]$. The background equation for the axion is

$$\partial_t^2 \, a_0(t) + m_a^2 \, a_0(t) = -g_{a\gamma\gamma} \, B_0 \, E_{0\parallel}(t) \ , \tag{4.1.2}$$

and for the photon

$$\partial_t \, E_{0\parallel}(t) = g_{a\gamma\gamma} \, B_0 \, [\partial_t \, a_0(t)] \ . \tag{4.1.3}$$

Since the scalar potential $\phi(t)$ equation has no source term

$$\Box \, \phi(t) = 0 \ , \tag{4.1.4}$$

we choose the radiation gauge

$$\phi(t) = 0 \ , \quad \nabla \cdot \vec{A}(\vec{x}) = 0 \ . \tag{4.1.5}$$

We can see from Eq. (4.1.3) that the axion oscillation induces the electric field, which is parallel to the direction of the background magnetic field.

$$E_{0\parallel}(t) = g_{a\gamma\gamma} \, B_0 \, a_0(t) \ . \tag{4.1.6}$$

Substituting Eq. (4.1.6) into Eq. (4.1.2), we can get

$$\ddot{a}_0(\tau) + \Omega_\beta^2 \, a_0(\tau) = 0 \ , \tag{4.1.7}$$

where we replace the variable t with $\tau \equiv m_a t$, and express a derivative with respect to τ by a dot. Here, we also introduced new dimensionless parameters β and Ω_β as follows:

$$\beta \equiv \frac{g_{a\gamma\gamma} \, B_0}{m_a} = 1.95 \times 10^{-9} \left(\frac{10^{-22} \, \mathrm{eV}}{m_a} \right) \left(\frac{g_{a\gamma\gamma}}{10^{-11} \, \mathrm{GeV}^{-1}} \right) \left(\frac{B_0}{10^{-9} \, \mathrm{G}} \right) \ , \tag{4.1.8}$$

$$\Omega_\beta \equiv \sqrt{1 + \beta^2} \ . \tag{4.1.9}$$

As a result, there are uniform static magnetic field, oscillating axion field and oscillating electric field in the background:

$$a_0(\tau) = \bar{a} \cos(\Omega_\beta \, \tau) \ , \tag{4.1.10}$$

$$E_{0\parallel}(\tau) = m_a \beta \, \bar{a} \cos(\Omega_\beta \, \tau) \ . \tag{4.1.11}$$

We introduce energy density ρ which is the sum of axion and induced electric field:

$$\rho \equiv \frac{1}{2} (\partial_t \, a_0)^2 + \frac{1}{2} m_a^2 \, a_0^2 \Big|_{\mathrm{present}} + \frac{1}{2} \, E_{0\parallel}^2 = \frac{1}{2} \, \bar{a}^2 m_a^2 \, \Omega_\beta^2 \ , \tag{4.1.12}$$

then background energy density $\rho_{\rm BG}$ is given by

$$\rho_{\rm BG} \equiv \rho + \frac{1}{2} B_0^2 \ . \tag{4.1.13}$$

We determine the axion amplitude $\bar{a}$ by the energy density ρ,

$$\bar{a} = \frac{\sqrt{2\rho}}{m_a \Omega_\beta} \ . \tag{4.1.14}$$

Thus, we found the following expressions

$$a_0(\tau) = \frac{\sqrt{2\rho}}{m_a \, \Omega_\beta} \cos\left(\Omega_\beta \, \tau\right) \ , \tag{4.1.15}$$

$$E_{0\parallel}(\tau) = \frac{\beta\sqrt{2\rho}}{\Omega_\beta} \cos\left(\Omega_\beta \, \tau\right) \ . \tag{4.1.16}$$

4.2 Perturbative Equations

Now we deal with perturbative equations as follows: for the axion,

$$(\Box - m_a^2) \, \delta a = g_{a\gamma\gamma} \left[\delta\vec{E} \cdot \vec{B}_0 + \vec{E}_0 \cdot \delta\vec{B} \right] , \tag{4.2.1}$$

and for the photon,

$$\begin{cases} \Box \, \delta\phi = -g_{a\gamma\gamma} \vec{B}_0 \cdot (\nabla \delta a) \ , \\ \Box \, \delta\vec{A} = g_{a\gamma\gamma} \left[(\partial_t \, \delta a) \, \vec{B}_0 + (\partial_t \, a_0) \, \delta\vec{B} + (\nabla \, \delta a) \times \vec{E}_0 \right] \ . \end{cases} \tag{4.2.2}$$

These equations are given by linearizing Eq. (3.1.7) and Eq. (3.1.8). We consider the situation where the magnetic field has the only x component, and the propagating direction of the axion and the photon is the z-axis. In this case, the scalar potential equation has no source term

$$\Box \, \delta\phi(z,t) = 0 \ . \tag{4.2.3}$$

Thus, we can choose the radiation gauge

$$\delta\phi(z,t) = 0, \quad \nabla\delta\vec{A}(z,t) = 0 \ . \tag{4.2.4}$$

Here is the equation written with components,

$$(\Box - m_a^2)\delta a(z,t) = g_{a\gamma\gamma} \left[\delta E_\parallel(z,t) B_0 - E_{0\parallel}(t) \frac{\partial \, \delta A_\perp(z,t)}{\partial \, z} \right] \ , \tag{4.2.5}$$

$$\Box \, \delta A_\parallel(z,t) = g_{a\gamma\gamma} \left[\left[\partial_t \, \delta a(z,t)\right] B_0 - \left[\partial_t \, a_0(t)\right] \frac{\partial \, \delta A_\perp(z,t)}{\partial \, z} \right] \ , \tag{4.2.6}$$

$$\Box \, \delta A_\perp(z,t) = g_{a\gamma\gamma} \left[\left[\partial_t \, a_0(t)\right] \frac{\partial \, \delta A_\parallel(z,t)}{\partial z} + \frac{\partial \, \delta a(z,t)}{\partial z} E_{0\parallel}(t) \right] \ . \tag{4.2.7}$$

Due to the time dependent oscillating axion field, the time translational symmetry is broken, but the system still has the spatial translation invariance. Hence, it is useful to perform the Fourier transformation,

$$\delta a(z,t) = \int \frac{dk}{2\pi}\, \delta a(k,t)\, e^{ikz} \ , \tag{4.2.8}$$

$$\delta A_i(z,t) = \int \frac{dk}{2\pi}\, \delta A_i(k,t)\, e^{ikz} \ , \tag{4.2.9}$$

$$\delta E_i(z,t) = -\int \frac{dk}{2\pi}\, \left[\partial_t\, \delta A_i(k,t)\right]\, e^{ikz} \ , \tag{4.2.10}$$

where the subscript i denotes $\parallel$ or $\perp$. The equations are rewritten as follows:

$$\partial_t^2\, \delta a(k,t) + (k^2 + m_a^2)\, \delta a(k,t) = g_{a\gamma\gamma}\, B_0\, \left[\partial_t\, \delta A_\parallel(k,t)\right] + i\, g_{a\gamma\gamma}\, k\, E_{0\parallel}(t)\, \delta A_\perp(k,t) \ , \tag{4.2.11}$$

$$\partial_t^2\, \delta A_\parallel(k,t) + k^2\, \delta A_\parallel(k,t) = -g_{a\gamma\gamma}\, B_0\, \left[\partial_t\, \delta a(k,t)\right] + i\, g_{a\gamma\gamma}\, k\, \left[\partial_t\, a_0(t)\right]\, \delta A_\perp(k,t) \ , \tag{4.2.12}$$

$$\partial_t^2\, \delta A_\perp(k,t) + k^2\, \delta A_\perp(k,t) = -i\, g_{a\gamma\gamma}\, k\, \left[\partial_t\, a_0(t)\right]\, \delta A_\parallel(k,t) - i\, g_{a\gamma\gamma}\, k\, E_{0\parallel}(t)\, \delta a(k,t) \ . \tag{4.2.13}$$

In addition, substituting the background solutions Eq. (4.1.15) and Eq. (4.1.16), we get the following equations:

$$\delta\ddot{a}(k,\tau) + \left[1+\kappa^2\right]\, \delta a(k,\tau) = \, \beta\, \delta\dot{A}_\parallel(k,\tau) + i\frac{\beta\epsilon}{\Omega_\beta}\cos\left(\Omega_\beta\tau\right)\delta A_\perp(k,t) \ , \tag{4.2.14}$$

$$\delta\ddot{A}_\parallel\left(k,\tau\right) + \kappa^2\delta A_\parallel\left(k,\tau\right) = -\beta\, \delta\dot{a}(k,\tau) - i\epsilon\sin\left(\Omega_\beta\tau\right)\delta A_\perp(k,t) \ , \tag{4.2.15}$$

$$\delta\ddot{A}_\perp\left(k,\tau\right) + \kappa^2\delta A_\perp\left(k,\tau\right) = i\epsilon\sin\left(\Omega_\beta\tau\right)\delta A_\parallel\left(k,\tau\right) - i\frac{\beta\epsilon}{\Omega_\beta}\cos\left(\Omega_\beta\tau\right)\delta a(k,\tau) \ , \tag{4.2.16}$$

where we introduced dimensionless parameters κ and ϵ as follows:

$$\kappa \equiv \frac{k}{m_a} \ , \quad \epsilon \equiv \frac{g_{a\gamma\gamma}\sqrt{2\rho}\, k}{m_a^2} = \frac{g_{a\gamma\gamma}\sqrt{2\rho}}{m_a}\,\kappa \ . \tag{4.2.17}$$

From now on, for simplicity, we neglect higher order terms in β and ϵ. Taking into account only the first order in β and ϵ, we obtain

$$\delta\ddot{a}(k,\tau) + \left[1+\kappa^2\right]\, \delta a(k,\tau) = \beta\, \delta\dot{A}_\parallel(k,\tau) \ , \tag{4.2.18}$$

$$\delta\ddot{A}_\parallel\left(k,\tau\right) + \kappa^2\delta A_\parallel\left(k,\tau\right) = -\beta\, \delta\dot{a}(k,\tau) - i\,\epsilon\,\sin(\tau)\,\delta A_\perp\left(k,\tau\right) \ , \tag{4.2.19}$$

$$\delta\ddot{A}_\perp\left(k,\tau\right) + \kappa^2\,\delta A_\perp\left(k,\tau\right) = i\,\epsilon\,\sin(\tau)\,\delta A_\parallel\left(k,\tau\right) \ . \tag{4.2.20}$$

In the case of $\epsilon = 0$, Eqs. (4.2.18)–(4.2.20) describe the conventional axion photon conversion, seen in Chap. 3.

Taking the circular polarization basis

$$\vec{e}_{L/R} = \frac{1}{\sqrt{2}}\left[\vec{e}_\parallel \mp\, i\,\vec{e}_\perp\right] \ , \tag{4.2.21}$$

Eqs. (4.2.18)–(4.2.20) are rewritten as follows:

$$\delta\ddot{a}(k,\tau) + \left[1+\kappa^2\right]\,\delta a(k,\tau) = \frac{\beta}{\sqrt{2}}\,\left[\delta\dot{A}_L(k,\tau) + \delta\dot{A}_R(k,\tau)\right]\,, \tag{4.2.22}$$

$$\delta\ddot{A}_{L/R}\,(k,\tau) + \left[\,\kappa^2 \pm \epsilon\,\sin(\tau)\right]\,\delta A_{L/R}\,(k,\tau) = -\frac{\beta}{\sqrt{2}}\,\delta\dot{a}(k,\tau)\,. \tag{4.2.23}$$

In the case of $\beta = 0$, Eqs. (4.2.23) end up the Mathieu equation and describe photon propagation in the presence of only axion dark matter [96]. Here, we should mention the previous work [97]. They investigated a similar system, but they neglected the parametric resonance. In our study, we consider the Mathieu type terms and deal with their resonance instability.

4.3 Numerical Results

In this section, we show some numerical results. These are obtained by solving Eqs. (4.2.18)–(4.2.20), or equivalently Eqs. (4.2.22)–(4.2.23). They show parameter sets which bring instability. We followed the way which is employed for the ordinary Mathieu equation. In Appx. A, there is a quick review of the Mathieu equation.

It is known that the solutions of the Mathieu equation,

$$\ddot{x}(\tau) + \left[\kappa^2 \pm \epsilon\,\sin(\tau)\right]x(\tau) = 0\,,$$

can be stable or unstable, depending on dimensionless parameters, κ and ϵ. Pairs of parameters, κ and ϵ, are often illustrated on a plane. The boundary lines between stable and unstable extend from certain points on κ axis,

$$\bar{\kappa} \equiv \frac{n}{2}\quad (n = 1, 2, 3, \cdots)\,, \tag{4.3.1}$$

where we add a bar above the κ in order to indicate clearly that the value is on the κ axis ($\epsilon = 0$). Here, we also introduce another dimensionless parameter,

$$\chi \equiv \kappa - \bar{\kappa}\,. \tag{4.3.2}$$

In the case of the axion dark matter photon conversion, we also found that there are bifurcation points around Eq. (4.3.1) by repeating the numerical calculation. Moreover, we empirically found another condition of the bifurcation points,

$$\sqrt{1+\bar{\kappa}^2} + \bar{\kappa} = n\quad (n = 2, 3, 4, \cdots)\,. \tag{4.3.3}$$

Solving this with respect to $\bar{\kappa}$, we get the following relation:

$$\bar{\kappa} \equiv \frac{n^2-1}{2n}\quad (n = 2, 3, 4, \cdots)\,. \tag{4.3.4}$$

In the following, we fix the value $\beta = 0.1$ and depict $(\kappa - \epsilon)$ planes. It will be discussed in Sec. 4.5 whether this value is appropriate. Numerical results give the shaded area, and the analytical solutions are overlaid in red and blue. The derivation of the red and blue curves is postponed until the next Sec. 4.4.

4.3.1 Shift of Bifurcation Points

The figure 4.1 shows that bifurcation points of transition curves appear around $\bar{\kappa} = 1/2$ and 1. To be more precise, bifurcation points are shifted even on the κ axis ($\epsilon = 0$) due to the background magnetic field.

As can be seen from Fig. 4.1 (a), the starting point of transition curves $\bar{\kappa} \sim 1/2$ is shifted by the magnetic field as

$$\chi_{1/2,-} \equiv -\frac{\epsilon}{2} + \frac{\beta^2}{8} \ , \tag{4.3.5}$$

$$\chi_{1/2,+} \equiv \frac{\epsilon}{2} + \frac{\beta^2}{8} \ . \tag{4.3.6}$$

In the case of $\bar{\kappa} \sim 1$, Fig. 4.1 (b), the unstable region splits into two regions.

$$\chi_{-} \equiv -\frac{\epsilon^2}{24} \ , \tag{4.3.7}$$

$$\chi_{+} \equiv \frac{5\epsilon^2}{24} \ , \tag{4.3.8}$$

$$\chi_{1,-} \equiv -\frac{\epsilon^2}{24} + \frac{\beta^2}{2} \ , \tag{4.3.9}$$

$$\chi_{1,+} \equiv \frac{5\epsilon^2}{24} + \frac{\beta^2}{2} \ . \tag{4.3.10}$$

The first two curves are exactly the same as the conventional Mathieu equation; see Eq. (A.4.18) in Appx. A. On the other hand, the other two curves are shifted by the magnetic field β.

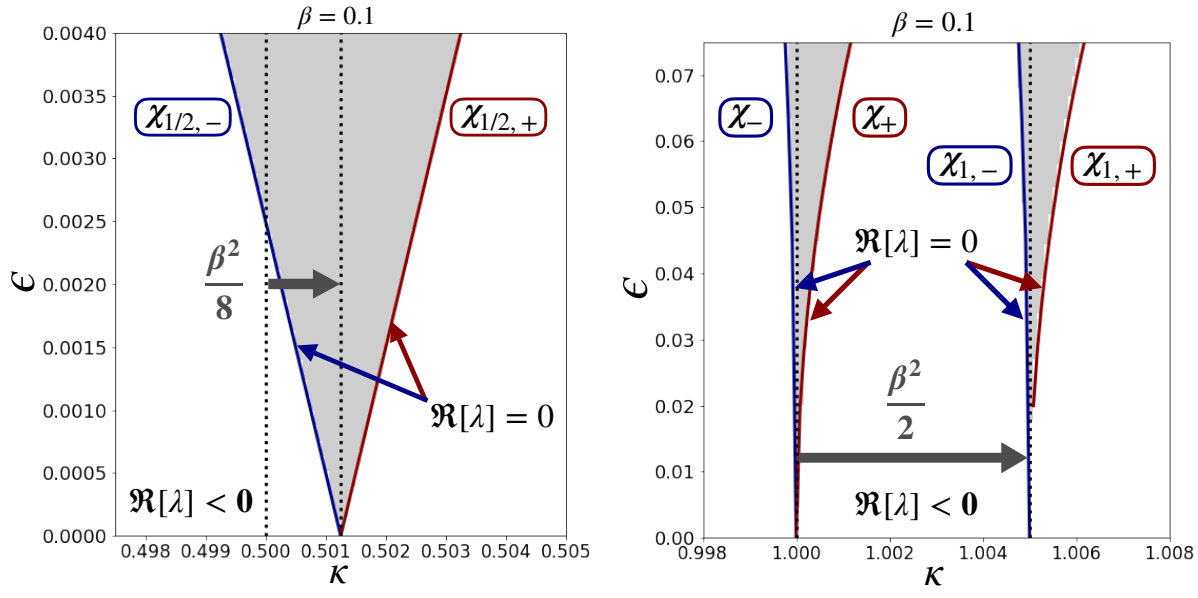

(a) $\bar{\kappa} = 1/2$ **(b)** $\bar{\kappa} = 1$

Figure 4.1: The Ince–Strutt charts. The shaded area represents parameter sets which make solutions of Eqs. (4.2.18)–(4.2.20) unstable.

4.3.2 New Bifurcation Points

The figure 4.2 shows the unstable region in the case of the condition Eq. (4.3.4) with $n = 2$. This instability is unique to the axion dark matter photon conversion. Here, we show only the analytical results, and the derivation process is explained in Sec. 4.4.

$$\chi_{3/4,\text{leading}} \equiv -\frac{5}{32}\beta^2 + \frac{\epsilon^2}{6} \ , \tag{4.3.11}$$

$$\chi_{3/4,-} \equiv \chi_{3/4,\text{leading}} - \frac{5}{48}\sqrt{15}\beta\epsilon^2 \ , \tag{4.3.12}$$

$$\chi_{3/4,+} \equiv \chi_{3/4,\text{leading}} + \frac{5}{48}\sqrt{15}\beta\epsilon^2 \ . \tag{4.3.13}$$

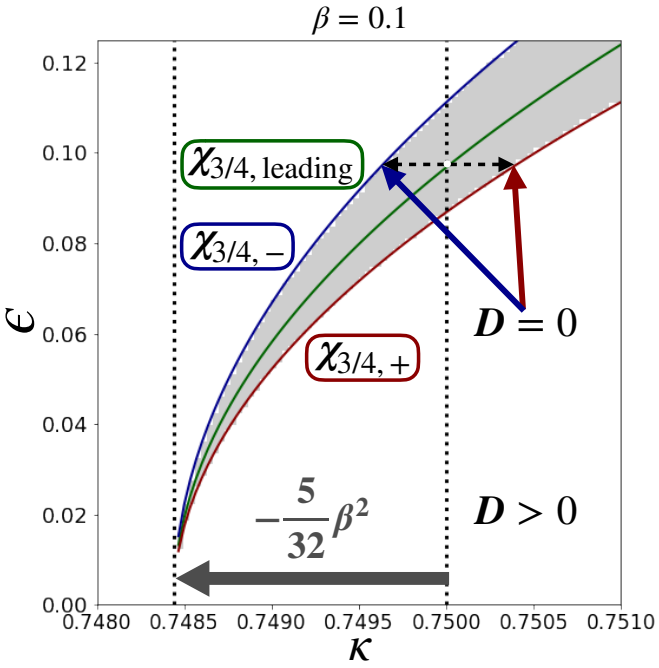

Figure 4.2: The Ince–Strutt chart in the case of $\bar{\kappa} = 3/4$. The shaded area represents parameter sets which make solutions of Eqs. (4.2.18)–(4.2.20) unstable. D in this figure means $D_{\text{up to next leading}}$ in Subsec. 4.4.3.

4.4 Analytical Interpretation

In this section, we provide an analytical understanding of numerical calculations, as shown in the previous section. The numerical results indicate that the mixing between axions and photons through background magnetic field increases the number of parameter sets which induce instability. From now, we derive the boundary lines which originate from Eq. (4.3.1) and Eq. (4.3.4) by treating parameters χ, β, ϵ as small quantity.

The basic equations (4.2.18)–(4.2.20) can be written as follows:

$$\ddot{\vec{x}} + B\,\dot{\vec{x}} + [K + E\sin(\tau)]\,\vec{x} = 0 \ , \tag{4.4.1}$$

by using a vector and matrices,

$$\vec{x} = \begin{bmatrix} \delta a(k,\tau) \\ \delta A_{\parallel}(k,\tau) \\ \delta A_{\perp}(k,\tau) \end{bmatrix}, \quad B = \begin{bmatrix} 0 & -\beta & 0 \\ \beta & 0 & 0 \\ 0 & 0 & 0 \end{bmatrix}, \quad K = \begin{bmatrix} 1+\kappa^2 & 0 & 0 \\ 0 & \kappa^2 & 0 \\ 0 & 0 & \kappa^2 \end{bmatrix}, \quad E = \begin{bmatrix} 0 & 0 & 0 \\ 0 & 0 & i\epsilon \\ 0 & -i\epsilon & 0 \end{bmatrix}. \tag{4.4.2}$$

Let us put an ansatz

$$\vec{x}(\tau) = e^{\lambda\tau} \left[\text{ The superpositions of many photon's overtones. } \right] ,$$

and substitute it into to Eq. (4.4.1). The coefficient matrix must vanish in order for Eq. (4.4.1) to have a nontrivial solution, *i.e.*, $\vec{x} \neq 0$. A new dimensionless parameter $\lambda \in \mathbb{C}$ is the growth rate, which satisfies $|\chi| \sim |\lambda| \ll 1$. The real part $\mathrm{Re}[\lambda]$ determines the stability of the solutions to Eq. (4.4.1), whereas the imaginary part $\mathrm{Im}[\lambda]$ detune the frequency of the solutions. The criteria for stable and unstable are given as follows:

$$\mathrm{Re}[\lambda] \leq 0 : \text{ stable}, \quad \mathrm{Re}[\lambda] > 0 : \text{ unstable}. \tag{4.4.3}$$

In the case of $\mathrm{Re}[\lambda] > 0$, the amplitude after one period T is approximately $e^{T\,\mathrm{Re}[\lambda]}$ times,

$$\vec{x}(\tau + T) \simeq e^{T\,\mathrm{Re}[\lambda]}\, \vec{x}(\tau) \ . \tag{4.4.4}$$

As one can see by actually calculating, the determinant of the coefficient matrix depends only on $q \equiv \lambda^2$. Therefore, it is more convenient to rewrite the criteria Eq. (4.4.3) to the condition for $q \equiv \lambda^2$,

$$\mathrm{Im}[q \equiv \lambda^2] = 0 \text{ and } \mathrm{Re}[q \equiv \lambda^2] \leq 0 : \text{ stable}, \quad \text{all other condition: unstable}. \tag{4.4.5}$$

Note that relative magnitude relationships among χ, β, ϵ, λ at each bifurcation points are different.

Before we go any further, we define the 3×3 matrices which compose the coefficient matrix:

$$\mathrm{Diag}(n) \equiv \lambda^2 I_3 + \lambda B + K - (\kappa n)^2\, I_3 \ , \tag{4.4.6}$$

$$\mathrm{Mix}(n) \equiv 4\kappa n \left[\frac{\lambda}{2}\, I_3 + \frac{B}{4} \right] \ , \tag{4.4.7}$$

where I_3 denotes the identity matrix, and n is a non-negative integer, $n = 0, 1, 2, \cdots$. The matrices K, B, E have already been defined in Eq. (4.4.2).

4.4.1 Shift of Bifurcation Point at $\bar{\kappa} = 1/2$

In the case of $\bar{\kappa} = 1/2$, we take the following ansatz

$$\vec{x}(\tau) = e^{\lambda\tau} \left[\vec{a}_1 \cos\left(\frac{\tau}{2}\right) + \vec{b}_1 \sin\left(\frac{\tau}{2}\right) \right] \ , \tag{4.4.8}$$

and see the hierarchy among parameters, $\lambda \sim \chi \sim \epsilon \sim \beta^2$, from numerical results. Hereafter, $\vec{a}_i$ and $\vec{b}_i$ $(i = 1, 2, \cdots)$ denote constant vector. Substituting Eq. (4.4.8) into Eq. (4.4.1), we obtain the 6×6 coefficient matrix $R_{1/2}(q, \chi, \beta, \epsilon)$,

$$R_{1/2}(q, \chi, \beta, \epsilon) \equiv \begin{bmatrix} \mathrm{Diag}(1) & \mathrm{Mix}(1) + E/2 \\ -\mathrm{Mix}(1) + E/2 & \mathrm{Diag}(1) \end{bmatrix} . \tag{4.4.9}$$

Evaluating the determinant of $R_{1/2}(q, \chi, \beta, \epsilon)$ at leading order, we obtain a quadratic equation with respect to $q \equiv \lambda^2$,

$$\left[q - \left(\sqrt{ - \left(\chi - \frac{\beta^2}{8} \right)^2 + \frac{\epsilon^2}{4} } + i \frac{\beta^2}{8} \right)^2 \right] \left[q - \left(\sqrt{ - \left(\chi - \frac{\beta^2}{8} \right)^2 + \frac{\epsilon^2}{4} } - i \frac{\beta^2}{8} \right)^2 \right] = 0 , \tag{4.4.10}$$

and four λs,

$$\lambda = \pm \sqrt{ - \left(\chi - \frac{\beta^2}{8} \right)^2 + \frac{\epsilon^2}{4} } \pm i \frac{\beta^2}{8} , \quad \pm \sqrt{ - \left(\chi - \frac{\beta^2}{8} \right)^2 + \frac{\epsilon^2}{4} } \mp i \frac{\beta^2}{8} . \tag{4.4.11}$$

Therefore, the range where the criterion for stability Eq. (4.4.3) is broken is as follows:

$$- \frac{\epsilon}{2} < \chi - \frac{\beta^2}{8} < \frac{\epsilon}{2} , \tag{4.4.12}$$

and the condition $\mathrm{Re}[\lambda] = 0$,

$$\chi - \frac{\beta^2}{8} = \pm \frac{\epsilon}{2} . \tag{4.4.13}$$

correspond to the boundary curves.

Here, we would like to comment on the growth rate Eq. (4.4.11). If one consider the situation where there is only coherent oscillating axion in the background like, *e.g.,* Ref. [96], then the growth rate does not depend on the axion mass m_a. In fact, one can confirm this by choosing $\beta = 0$ in Eq. (4.4.11). However, in our case $\beta \neq 0$, note that the growth rate $m_a \, \mathrm{Re}[\lambda]$ becomes to depend on the axion mass due to the presence of the background magnetic field β.

4.4.2 Shift of Bifurcation Point at $\bar{\kappa} = 1$

In the case of $\bar{\kappa} = 1$, we take the following ansatz

$$\vec{x}(\tau) = e^{\lambda \tau} \left[\vec{a}_1 \cos(\tau) + \vec{b}_1 \sin(\tau) + \vec{a}_2 \cos(2\tau) + \vec{b}_2 \sin(2\tau) + \vec{c} \right] , \tag{4.4.14}$$

and see the hierarchy among parameters, $\lambda \sim \chi \sim \epsilon^2 \sim \beta^2$, from numerical results. Substituting Eq. (4.4.14) into Eq. (4.4.1), we obtain the 15×15 coefficient matrix

$R_1(q,\chi,\beta,\epsilon)$,

$$R_1(q,\chi,\beta,\epsilon) \equiv \begin{bmatrix} \mathrm{Diag}(0) & 0 & E/2 & 0 & 0 \\ 0 & \mathrm{Diag}(1) & \mathrm{Mix}(1) & 0 & E/2 \\ E & -\mathrm{Mix}(1) & \mathrm{Diag}(1) & -E/2 & 0 \\ 0 & 0 & -E/2 & \mathrm{Diag}(2) & \mathrm{Mix}(2) \\ 0 & E/2 & 0 & -\mathrm{Mix}(2) & \mathrm{Diag}(2) \end{bmatrix} . \tag{4.4.15}$$

Evaluating the determinant of $R_1(q,\chi,\beta,\epsilon)$ at leading order, we obtain a quadratic equation with respect to $q \equiv \lambda^2$,

$$\left[q + \left(\chi + \frac{\epsilon^2}{24}\right)\left(\chi - \frac{5\epsilon^2}{24}\right)\right]\left[q + \left(\chi - \frac{\beta^2}{2} + \frac{\epsilon^2}{24}\right)\left(\chi - \frac{\beta^2}{2} - \frac{5\epsilon^2}{24}\right)\right] = 0 \, . \tag{4.4.16}$$

Therefore, the range where the criterion for stability Eq. (4.4.3) is broken is as follows:

$$-\frac{\epsilon^2}{24} < \chi < \frac{5\epsilon^2}{24} \, , \; -\frac{\epsilon^2}{24} < \chi - \frac{\beta^2}{2} < \frac{5\epsilon^2}{24} \, , \tag{4.4.17}$$

and the condition $\mathrm{Re}[\lambda] = 0$,

$$\chi = -\frac{\epsilon^2}{24}, \;\; \frac{5\epsilon^2}{24} \, , \;\; \frac{\beta^2}{2} - \frac{\epsilon^2}{24}, \;\; \frac{\beta^2}{2} + \frac{5\epsilon^2}{24} \, , \tag{4.4.18}$$

correspond to the boundary curves.

4.4.3 A New Bifurcation Point at $\bar{\kappa} = 3/4$

The unstable region around $\bar{\kappa} = 3/4$ is unique to the axion dark matter photon conversion. We take the following ansatz

$$\vec{x}(\tau) = e^{\lambda\tau} \begin{bmatrix} \vec{a}_1 \cos(\tau/4) + \vec{b}_1 \sin(\tau/4) + \vec{a}_2 \cos(3\tau/4) + \vec{b}_2 \sin(3\tau/4) \\ + \vec{a}_3 \cos(5\tau/4) + \vec{b}_3 \sin(5\tau/4) + \vec{a}_4 \cos(7\tau/4) + \vec{b}_4 \sin(7\tau/4) \end{bmatrix} \, , \tag{4.4.19}$$

and see the hierarchy among parameters, $\lambda \sim \chi \sim \epsilon^2 \sim \beta^2$, from numerical results. Substituting Eq. (4.4.19) into Eq. (4.4.1), we obtain the 24×24 coefficient matrix $R_{3/4}(q,\chi,\beta,\epsilon)$,

$$
\begin{aligned}
&R_{3/4}(q,\chi,\beta,\epsilon) \\
&\equiv \begin{bmatrix}
\mathrm{Diag}_{3/4}(0) & \mathrm{Mix}_{3/4}(0) & 0 & E/2 & 0 & E/2 & 0 & 0 \\
-\mathrm{Mix}_{3/4}(0) & \mathrm{Diag}_{3/4}(0) & E/2 & 0 & -E/2 & 0 & 0 & 0 \\
0 & E/2 & \mathrm{Diag}_{3/4}(1) & \mathrm{Mix}_{3/4}(1) & 0 & 0 & 0 & E/2 \\
E/2 & 0 & -\mathrm{Mix}_{3/4}(1) & \mathrm{Diag}_{3/4}(1) & 0 & 0 & -E/2 & 0 \\
0 & -E/2 & 0 & 0 & \mathrm{Diag}_{3/4}(2) & \mathrm{Mix}_{3/4}(2) & 0 & 0 \\
E/2 & 0 & 0 & 0 & -\mathrm{Mix}_{3/4}(2) & \mathrm{Diag}_{3/4}(2) & 0 & 0 \\
0 & 0 & 0 & -E/2 & 0 & 0 & \mathrm{Diag}_{3/4}(3) & \mathrm{Mix}_{3/4}(3) \\
0 & 0 & E/2 & 0 & 0 & 0 & -\mathrm{Mix}_{3/4}(3) & \mathrm{Diag}_{3/4}(3)
\end{bmatrix} .
\end{aligned}
\tag{4.4.20}
$$

Note that in this case, the definition of matrices are different from Eq. (4.4.6) and Eq. (4.4.7),

$$
\mathrm{Diag}_{3/4}(n) \equiv \lambda^2 I_3 + \lambda B + K - \left(\frac{2n+1}{4}\right)^2 I_3 \ , \tag{4.4.21}
$$

$$
\mathrm{Mix}_{3/4}(n) \equiv (2n+1)\left[\frac{\lambda}{2} I_3 + \frac{B}{4}\right] \ . \tag{4.4.22}
$$

Evaluating the determinant of $R_{3/4}(q,\chi,\beta,\epsilon)$ at leading order, we obtain a cubic equation with respect to $q \equiv \lambda^2$,

$$
\left[q + \frac{9}{25}\left(\chi + \frac{25}{24}\beta^2\right)^2\right]\left[q + \left(\chi - \frac{3}{8}\beta^2 - \frac{4}{15}\epsilon^2\right)^2\right]\left[q + \left(\chi - \frac{4}{15}\epsilon^2\right)^2\right] = 0 \ . \tag{4.4.23}
$$

and the solutions,

$$
q_1 \equiv -\frac{9}{25}\left(\chi + \frac{25}{24}\beta^2\right)^2 \ , \tag{4.4.24}
$$

$$
q_2 \equiv -\left(\chi - \frac{3}{8}\beta^2 - \frac{4}{15}\epsilon^2\right)^2 \ , \tag{4.4.25}
$$

$$
q_3 \equiv -\left(\chi - \frac{4}{15}\epsilon^2\right)^2 \ . \tag{4.4.26}
$$

The equation (4.4.23) has three negative real solutions q_1, q_2, q_3; that is, λ must be pure imaginary. Thus, the condition $\mathrm{Re}[\lambda] = 0$, which has given boundaries in the case of Subsec. 4.4.1 and Subsec. 4.4.2, is now automatically satisfied. This means that the boundary is determined by another condition in the case of $\bar{\kappa} = 3/4$. As a side note, no boundary line can be obtained from the condition $q = 0$,

$$
\chi = -\frac{25}{24}\beta^2 \ , \quad \frac{3}{8}\beta^2 + \frac{4}{15}\epsilon^2 \ , \quad \frac{4}{15}\epsilon^2 \ . \tag{4.4.27}
$$

We need to find a condition specific to $\bar{\kappa} = 3/4$, which leads to its boundary lines. Then, we focused on higher-order contributions. This idea is explained below. We refer to the discriminant of the cubic equation (4.4.23) as D_{leading}. The equation (4.4.23) says $D_{\text{leading}} \geq 0$ as long as the determinant of the coefficient matrix is evaluated at leading order. In the case of $D_{\text{leading}} > 0$, if we evaluate the determinant of $R_{3/4}(q, \chi, \beta, \epsilon)$ up to the next leading order, we still cannot obtain boundary lines. This is because the sign of discriminant is never inverted. However, after imposing the condition $D_{\text{leading}} = 0$ on Eq. (4.4.23), the situation could change due to higher contributions. In other words, the discriminant of the cubic equation obtained by evaluating the determinant up to the next leading order could be negative. This creates a parameter region which violates the stability condition Eq. (4.4.5), as it appeared in the result of the numerical calculation Fig. 4.2.

Now, let us carry out what was said above. First, we impose the condition $D_{\text{leading}} = 0$. There are three possibilities:

$$q_1 = q_2 \ , \quad \text{or} \quad q_2 = q_3 \ , \quad \text{or} \quad q_3 = q_1 \ .$$

Since it is expected that instability around $\bar{\kappa} = 3/4$ is caused by the coupling of the axion and the photon ($\|$-component) through the magnetic field, $q_1 = q_2$ seems to be plausible. Solving the equation

$$-\frac{9}{25}\left(\chi + \frac{25}{24}\beta^2\right)^2 = -\left(\chi - \frac{3}{8}\beta^2 - \frac{4}{15}\epsilon^2\right)^2 , \tag{4.4.28}$$

we obtain the relation among parameters,

$$\chi = -\frac{5}{32}\beta^2 + \frac{\epsilon^2}{6} \ . \tag{4.4.29}$$

On the curve which satisfies this relationship Eq. (4.4.29), the cubic equation (4.4.23) can be rewritten,

$$[\, q + f_1(\beta, \epsilon)\,]\,[\, q + f_2(\beta, \epsilon)\,]^2 = 0 \ , \tag{4.4.30}$$

and it has multiple root $q = -f_2(\beta, \epsilon)$, where $f_1(\beta, \epsilon)$ and $f_2(\beta, \epsilon)$ are positive real functions. As far as we consider only the leading order, we cannot find the parameter region which violates the stability condition Eq. (4.4.5).

Then, we proceed to the next leading order. There are concrete expressions in Appx. B. The determinant at the next leading order $\det[R_{3/4}(q, \chi, \beta, \epsilon)]_{\text{next leading}}$ is also a cubic equation. Up to the next leading order, we have

$$\begin{aligned} &\det[R_{3/4}(q, \chi, \beta, \epsilon)]_{\text{up to next leading}} \\ &\quad \equiv \det[R_{3/4}(q, \chi, \beta, \epsilon)]_{\text{leading}} + \det[R_{3/4}(q, \chi, \beta, \epsilon)]_{\text{next leading}} \\ &\quad \equiv C_3(\chi, \beta, \epsilon)q^3 + C_2(\chi, \beta, \epsilon)q^2 + C_1(\chi, \beta, \epsilon)q + C_0(\chi, \beta, \epsilon) = 0 \ , \end{aligned} \tag{4.4.31}$$

where we labeled the coefficients of each order of q as C_3, C_2, C_1, C_0. The discriminant of the cubic equation (4.4.31) is given by

$$\begin{aligned} D_{\text{up to next leading}}(\chi, \beta, \epsilon) \equiv &- 4C_3(\chi, \beta, \epsilon)[C_1(\chi, \beta, \epsilon)]^3 - 27[C_3(\chi, \beta, \epsilon)]^2[C_0(\chi, \beta, \epsilon)]^2 \\ &+ [C_2(\chi, \beta, \epsilon)]^2[C_1(\chi, \beta, \epsilon)]^2 - 4[C_2(\chi, \beta, \epsilon)]^3 C_0(\chi, \beta, \epsilon) \\ &+ 18C_3(\chi, \beta, \epsilon)C_2(\chi, \beta, \epsilon)C_1(\chi, \beta, \epsilon)C_0(\chi, \beta, \epsilon) \ . \end{aligned} \tag{4.4.32}$$

Let us find a correction term X,

$$\chi = -\frac{5}{32}\beta^2 + \frac{\epsilon^2}{6} + X \ , \tag{4.4.33}$$

arising from higher order contribution to Eq. (4.4.29). On this curve Eq. (4.4.33), the cubic equation (4.4.31) will have multiple roots. The correction X is given by

$$D_{\text{up to next leading}} \left(-\frac{5}{32}\beta^2 + \frac{\epsilon^2}{6} + X, \beta, \epsilon \right) \Big|_{\text{leading}} = 0 \ . \tag{4.4.34}$$

In the end, we obtain a particular relation among parameters up to the next leading order,

$$\chi = -\frac{5}{32}\beta^2 + \frac{\epsilon^2}{6} \pm \frac{5}{48}\sqrt{15}\beta\epsilon^2 \ . \tag{4.4.35}$$

The equation (4.4.35) shows that Eq. (4.4.29) splits into two curves. In the region which intervenes between these curves, the all order of the discriminant $D_{\text{up to next leading}}$ is negative, *i.e.,* $D_{\text{up to next leading}} < 0$. Hence, in this region, the cubic equation (4.4.31) can be rewritten as follows:

$$[\, q + g_1(\beta, \epsilon) \,] \, [\, q + h_1(\beta, \epsilon) + i h_2(\beta, \epsilon) \,] \, [\, q + h_1(\beta, \epsilon) - i h_2(\beta, \epsilon) \,] = 0 \ , \tag{4.4.36}$$

and the criterion for stability Eq. (4.4.5) is not satisfied, where h_i and g_i $(n = 1, 2)$ are positive real functions. Thus, we have found that two curves Eq. (4.4.35) are just the transition curves for $\bar{\kappa} = 3/4$.

4.5 Discussion

Finally, let us consider what kind of system needs to be arranged to give rise to instability, which we have seen in Subsec. 4.3.2 and Subsec. 4.4.3. A plausible value depends on the wavelength L_{wave},

$$L_{\text{wave}} \equiv \frac{2\pi}{k} \ . \tag{4.5.1}$$

The dimensionless parameter κ determines a relation between the axion mass and the wavelength of electromagnetic waves. The parameter β characterizes the strength of magnetic fields. The value of ϵ is determined at the very end, after the values of κ and β are fixed. The question is whether both the conversion and the resonance can be important at the same time.

In the case of radio waves, three parameters included in basic equations (4.2.18)–(4.2.20) are given as follows:

$$\kappa = 0.75 \left(\frac{1.65 \times 10^{-14}\,\text{eV}}{m_a} \right) \left(\frac{10^{10}\,\text{cm}}{L} \right) \ , \tag{4.5.2}$$

$$\beta = 0.12 \left(\frac{1.65 \times 10^{-14}\,\text{eV}}{m_a} \right) \left(\frac{g_{a\gamma\gamma}}{10^{-11}\,\text{GeV}^{-1}} \right) \left(\frac{B_0}{10^{7}\,\text{G}} \right) \ , \tag{4.5.3}$$

$$\epsilon = 0.097 \left(\frac{\kappa}{0.75} \right) \left(\frac{g_{a\gamma\gamma}}{10^{-11}\,\text{GeV}^{-1}} \right) \left(\frac{1.65 \times 10^{-14}\,\text{eV}}{m_a} \right) \left(\sqrt{\frac{\rho}{0.3 \times 10^{16}\,\text{GeV/cm}^3}} \right) \ . \tag{4.5.4}$$

A strong magnetic field $B_0 \sim 10^7\,\mathrm{G}$ can be realized with a white dwarf. However, energy density ρ needs 10^{16} times as much as the average density of dark matter near the solar system.

In the case of an ultralight axion, three parameters included in basic equations (4.2.18)–(4.2.20) are given as follows:

$$\kappa = 0.75 \left(\frac{1.65 \times 10^{-22}\,\mathrm{eV}}{m_a}\right) \left(\frac{10^{18}\,\mathrm{cm}}{L}\right) , \tag{4.5.5}$$

$$\beta = 0.12 \left(\frac{1.65 \times 10^{-22}\,\mathrm{eV}}{m_a}\right) \left(\frac{g_{a\gamma\gamma}}{10^{-11}\,\mathrm{GeV}^{-1}}\right) \left(\frac{B_0}{10^{-1}\,\mathrm{G}}\right) , \tag{4.5.6}$$

$$\epsilon = 0.097 \left(\frac{\kappa}{0.75}\right) \left(\frac{g_{a\gamma\gamma}}{10^{-11}\,\mathrm{GeV}^{-1}}\right) \left(\frac{1.65 \times 10^{-22}\,\mathrm{eV}}{m_a}\right) \left(\sqrt{\frac{\rho}{0.3\,\mathrm{GeV/cm}^3}}\right) . \tag{4.5.7}$$

It might be difficult to find the astrophysical situation with the strength of magnetic fields, $B_0 = 10^{-1}\,\mathrm{G}$ and to detect electromagnetic waves $L = 10^{18}\,\mathrm{cm} \sim 1\,\mathrm{pc}$.

Devising a smart way, we may be able to realize the situation where both the axion dark matter photon conversion and the resonance are relevant in the Universe or in the laboratory. We leave such a concrete physical application to future work.

Chapter 5

Conclusion

In this thesis, we have studied the conversion phenomena of the axion dark matter. The axion photon conversion induced by a static constant magnetic field has been studied in various situations so far. These previous studies pointed out that the axion photon conversion could bring interesting consequences to observations. Therefore, the conversion signal has the potential to bring us information about undiscovered axions and the magnetic fields in the Universe.

The axion is also known as a leading candidate for the dark matter. In other words, there is a possibility that the coherent oscillations of axions make up for the energy density of the dark matter. As behind this, we can mention facts that the LHC experiment has no signal of supersymmetric particles and that cold dark matter, which is successful on the cosmological scale, may have a defect below the galactic scale. If the axion is the true identity of dark matter, then these facts are very compatible. Moreover, axions have a large parameter space which is not yet sufficiently restricted.

Taking the above into account, it is worth considering the axion photon system in which there are not only a static magnetic field but also an oscillating axion in the background. First, we have prepared the fundamental equations. These equations are composed of both conventional conversion terms and the Mathieu type terms. Second, by applying knowledge about the Mathieu equation and using numerical calculation, we have classified parameters in the fundamental equations into those which make the solution stable and unstable. As a result, we have found a characteristic unstable condition which the conventional Mathieu equation does not have. Third, we have also provided analytical interpretations of the obtained numerical results. Specifically, by treating parameters as small quantities, we have analytically derived the location and the width of the unstable region appearing in the parameter plane. This is useful when we choose an appropriate physical setup in order to study the effects of our system on the observations. Finally, we have also briefly considered the existence of such a suitable physical setup, but it has turned out that, in naive situations, we cannot observe the characteristic signal of our system. We leave this point to future work.

Acknowledgment

I am really indebted to my supervisor Jiro Soda for his valuable advice throughout my Ph.D. program. I gratefully acknowledge Arata Aoki for fruitful discussions and collaborations, and Toshifumi Noumi for continuous encouragement. Thanks are also due to all colleagues and alumni of the Institute of Cosmophysics and Particle Theory Group in Kobe University. In addition, I am always grateful for my family's support. Without their help, this thesis would never have been possible.

This work was in part supported by JSPS KAKENHI Grant No. JP18J20018. I was also supported by JSPS Bilateral Joint Research Projects (JSPS-NRF Collaboration) String Axion Cosmology.

Appendix A

The Mathieu Equation in a Nutshell

In this appendix, we provide a quick review of the Mathieu equation. There is no mathematically rigorous discussion. For mathematical proofs and more details, please refer to the reference appropriately, *e.g.*, Refs. [98–101].

A.1 The Floquet Theory

In this section, we deal with the following system of first-order differential equations,

$$\dot{\vec{x}} = \mathbf{P}(\tau)\,\vec{x}\ , \quad \mathbf{P}(\tau+T) = \mathbf{P}(\tau)\ , \tag{A.1.1}$$

where $\mathbf{P}(\tau)$ is a $n \times n$ matrix with its period T, and we express a derivative with respect to τ by a dot. The solutions of Eq. (A.1.1) is generally not a periodic except the trivial case, $\vec{x} = 0$.

The Floquet's theorem [102] says that Eq. (A.1.1) has at least one non-trivial solution such that

$$\vec{y}_i(\tau+T) = \mu_i \vec{y}_i(\tau), \quad i = 1, 2, \cdots n\ , \tag{A.1.2}$$

where $\mu_i \in \mathbb{C}$ is a constant and what is called the **characteristic multiplier**. This solution Eq. (A.1.2) is called a **normal solution.**

In the following, we will explain how μ_i can be obtained. Before that, we introduce the **fundamental matrix**

$$\mathbf{\Phi}(\tau) = \left[\vec{\phi}_1, \vec{\phi}_2, \cdots \vec{\phi}_n\right]\ , \tag{A.1.3}$$

where $\vec{\phi}_1, \vec{\phi}_2, \cdots \vec{\phi}_n$ are linearly independent solutions of Eq. (A.1.1). In particular, $\mathbf{\Phi}_0(\tau)$ denotes one with the initial condition $\mathbf{\Phi}(0) = \mathbf{I}_n$, where $\mathbf{I}_n$ is an identity matrix of size n. Since the column vector of $\mathbf{\Phi}_0(\tau)$ are linearly independent, we can expand a matrix $\mathbf{\Phi}(\tau)$, which is constructed by arranging the solutions under another initial condition,

$$\mathbf{\Phi}(\tau) = \mathbf{\Phi}_0(\tau)\mathbf{C}\ , \tag{A.1.4}$$

where $\mathbf{C}$ is a constant matrix. If one choose $\mathbf{\Phi}_0(\tau+T)$ as $\mathbf{\Phi}(\tau)$, $\mathbf{\Phi}_0(\tau+T)$ can be written in the following form,

$$\mathbf{\Phi}_0(\tau+T) = \mathbf{\Phi}_0(\tau)\mathbf{C}\ . \tag{A.1.5}$$

Substituting $\tau = 0$, we can get,

$$\mathbf{C} = \mathbf{\Phi}_0(T) \ , \tag{A.1.6}$$

and

$$\mathbf{\Phi}_0(nT) = \mathbf{C}^n \ . \tag{A.1.7}$$

This shows that the matrix $\mathbf{C}$ determines the stability of the solution.

Now, we consider another fundamental matrix $\mathbf{\Phi}_y$ by transforming bases. We can expand $\mathbf{\Phi}_y$ with $\mathbf{\Phi}_0$ again,

$$\mathbf{\Phi}_y(\tau) = \mathbf{\Phi}_0(\tau)\mathbf{C}_y \ . \tag{A.1.8}$$

Then, we obtain

$$\begin{aligned} \mathbf{\Phi}_y(\tau + T) &= \mathbf{\Phi}_0(\tau + T)\mathbf{C}_y \ , \\ &= \mathbf{\Phi}_0(\tau)\mathbf{C}\mathbf{C}_y \ , \\ &= \mathbf{\Phi}_y(\tau)\mathbf{C}_y^{-1}\mathbf{C}\mathbf{C}_y \ . \end{aligned} \tag{A.1.9}$$

Here, if one select the matrix obtained by arranging the eigenvectors of the matrix $\mathbf{C}$ as the $\mathbf{C}_y$, the matrix $\mathbf{C}_y^{-1}\mathbf{C}\mathbf{C}_y$ is diagonalized with the eigenvalues μ_i of the matrix $\mathbf{C}$ on its main diagonal. Then, $\mathbf{\Phi}_y(\tau + T)$ is also diagonalized. If one write the column vector of the matrix $\mathbf{\Phi}_y(\tau)$ as $y_i(t)$, we obtain the solution described above,

$$\vec{y_i}(\tau + T) = \mu_i \vec{y_i}(\tau) \ . \tag{A.1.2}$$

Therefore, the eigenvalues of the matrix Eq. (A.1.6) tell us the stability of the solution for Eq. (A.1.1). If $|\mu_i| > 1$, then $\vec{y_i}$ diverge when $\tau \to \infty$, whereas if $|\mu_i| < 1$, then $\vec{y_i} \to 0$ when $\tau \to \infty$. If every eigenvalue of the matrix $\mathbf{C}$ Eq. (A.1.6) satisfies the condition $|\mu_i| < 1$, the system Eq. (A.1.1) is stable; that is, all solutions are bounded. On the other hand, if there is at least one eigenvalue which satisfies $|\mu_i| > 1$, the system Eq. (A.1.1) is unstable; that is, an unbounded solution exists.

The point of Floquet's theorem is that it implies the existence of a periodic solution when we choose a special number as a characteristic multiplier. To see this, we define a **characteristic exponent** ρ

$$e^{\rho_i T} \equiv \mu_i \ . \tag{A.1.10}$$

By using this quantity, normal solutions are written as the following form

$$\vec{y_i}(\tau) = \vec{p_i}(\tau)e^{\rho_i \tau} \ , \tag{A.1.11}$$

where $\vec{p}(\tau)$ is a vector function with a period T. If one replace variable τ by $\tau + T$,

$$\vec{y_i}(\tau + T) = \vec{p_i}(\tau)e^{\rho_i \tau}e^{\rho_i T} \ , \tag{A.1.12}$$

and if the matrix $\mathbf{C}$ has an eigenvalue $\mu_i = 1$, then a periodic solution exist with a period T. This can be seen from Eq. (A.1.2). Besides this, whenever $\mathbf{C}$ has an eigenvalue like

$$\mu_i = 1^{1/m}, \quad m\text{: a positive integer}, \tag{A.1.13}$$

there are periodic solutions with a period mT.

At the end of the section, we give a relation which holds in the system Eq. (A.1.1),

$$\mu_1\mu_2\cdots\mu_n = \exp\left(\int_0^T \mathrm{tr}\left[\mathbf{P}(s)\right] ds\right), \tag{A.1.14}$$

without proof.

A.2 The Mathieu Equation

The Mathieu equation

$$\ddot{x} + \left[\omega_0^2 + \delta \sin(\tau)\right] x = 0, \tag{A.2.1}$$

was first introduced by French mathematician Émile Mathieu in 1868 [103], where ω_0 and δ are parameters, and they do not have to small value. This equation represents a harmonic oscillator whose frequency also oscillates. Since the Mathieu equation can be rewritten as

$$\frac{d}{d\tau}\begin{bmatrix} x \\ v \end{bmatrix} = \begin{bmatrix} 0 & 1 \\ -\omega_0^2 - \delta \sin(\tau) & 0 \end{bmatrix} \begin{bmatrix} x \\ v \end{bmatrix}, \tag{A.2.2}$$

it fits to the case of Eq. (A.1.1), where $v \equiv \dot{x}$. In this case, the matrix $\mathbf{P}(\tau)$ is defined as

$$\mathbf{P}(\tau) = \begin{bmatrix} 0 & 1 \\ -\omega_0^2 - \delta \sin(\tau) & 0 \end{bmatrix}, \tag{A.2.3}$$

with its period 2π. Thus, we get a relation from Eq. (A.1.14):

$$\mu_1 \mu_2 = 1 \ . \tag{A.2.4}$$

Now, we consider a fundamental matrix $\mathbf{\Phi}_0$ which consist of two solution vectors $\begin{bmatrix} \phi_{11}(\tau) \\ \phi_{21}(\tau) \end{bmatrix}$ and $\begin{bmatrix} \phi_{12}(\tau) \\ \phi_{22}(\tau) \end{bmatrix}$ with the initial conditions:

$$\begin{bmatrix} \phi_{11}(0) \\ \phi_{21}(0) \end{bmatrix} = \begin{bmatrix} 1 \\ 0 \end{bmatrix}, \quad \begin{bmatrix} \phi_{12}(0) \\ \phi_{22}(0) \end{bmatrix} = \begin{bmatrix} 0 \\ 1 \end{bmatrix} . \tag{A.2.5}$$

Two characteristic multipliers, μ_1 and μ_2, are derived as eigenvalues of the matrix $\mathbf{C}$

$$\mathbf{C} = \begin{bmatrix} \phi_{11}(2\pi) & \phi_{12}(2\pi) \\ \phi_{21}(2\pi) & \phi_{22}(2\pi) \end{bmatrix} \ : \tag{A.2.6}$$

that is, we solve the equation

$$\mu^2 - (\operatorname{tr} \mathbf{C})\mu + \det \mathbf{C} = 0, \tag{A.2.7}$$

where $\det \mathbf{C} = 1$ from Eq. (A.2.4). Thus, we obtain

$$\mu = \frac{\operatorname{tr} \mathbf{C} \pm \sqrt{(\operatorname{tr} \mathbf{C})^2 - 4}}{2} = \frac{\phi_{11}(2\pi) + \phi_{22}(2\pi) \pm \sqrt{\left[\phi_{11}(2\pi) + \phi_{22}(2\pi)\right]^2 - 4}}{2} \ . \tag{A.2.8}$$

The $\operatorname{tr} \mathbf{C}$ depends on the parameter of Eq. (A.2.1), ω_0 and δ.

- $\mathrm{tr}\,\mathbf{C} > 2$

In this case, characteristic multipliers are real, positive and $\mu_1 \neq \mu_2$. They are a reciprocal number with each other,

$$\mu_2 = \frac{1}{\mu_1} \ . \tag{A.2.9}$$

The corresponding characteristic exponents are written as follows:

$$\rho_1 = \sigma > 0, \quad \rho_2 = -\sigma < 0 \ , \tag{A.2.10}$$

where σ is a real constant. Assuming that $c_i\,(i = 1, 2)$ are constants and $\vec{p}_i\,(i = 1, 2)$ are vector functions with period 2π, the general solution is given by,

$$\vec{x}(\tau) = c_1 e^{\sigma\tau}\vec{p}_1(\tau) + c_2 e^{-\sigma\tau}\vec{p}_2(\tau) \ . \tag{A.2.11}$$

Therefore, in this parameter region $\mathrm{tr}\,\mathbf{C} > 2$, there are unbounded solutions.

- $\mathrm{tr}\,\mathbf{C} = 2$

In this case, $\mu_1 = \mu_2 = 1$ then $\rho_1 = \rho_2 = 0$. Thus, from Eq. (A.1.2), there is one solution of period 2π on the curve $\mathrm{tr}\,\mathbf{C} = 2$.

- $-2 < \mathrm{tr}\,\mathbf{C} < 2$

In this case, the characteristic multipliers $\mu_i \in \mathbb{C}$ are complex conjugate with each other. Since the absolute value should be $|\mu_i| = 1$, characteristic exponents turn out $\rho_1 = i\nu, \rho_2 = -i\nu$, where ν is a real positive number. The general solution is given by,

$$\vec{x}(\tau) = c_1 e^{i\nu\tau}\vec{p}_1(\tau) + c_2 e^{-i\nu\tau}\vec{p}_2(\tau) \ . \tag{A.2.12}$$

All solutions in this parameter region are bounded, however, they are not periodic but *quasi* periodic. This is because there are two frequencies ν and 2π; see also Fig. A.2.

- $\mathrm{tr}\,\mathbf{C} = -2$

In this case, $\mu_1 = \mu_2 = -1$ then $\rho_1 = \rho_2 = i/2$. Thus, from Eq. (A.1.2), there is one solution with the period 4π on the curve $\mathrm{tr}\,\mathbf{C} = -2$.

- $\mathrm{tr}\,\mathbf{C} < -2$

In this case, characteristic multipliers are real and negative and $\mu_1 \neq \mu_2$. The general solution is given by,

$$\vec{x}(\tau) = c_1 e^{\left(\sigma+\frac{i}{2}\right)\tau}\vec{p}_1(\tau) + c_2 e^{-\left(\sigma+\frac{i}{2}\right)\tau}\vec{p}_2(\tau) \ . \tag{A.2.13}$$

A.3 The Ince–Strutt Chart

In Appx. A.1, we saw that the characteristic multiplier μ_i determines the stability of the solution for Eq. (A.1.1). However, in general, it is difficult to obtain $\mathbf{\Phi}_0$ analytically. In fact, it is often adopted numerical integration in order to obtain $\mathbf{\Phi}_0$.

We numerically calculated the matrix $\mathbf{\Phi}_0$ at each point (ω_0, δ), and comprehensively investigated whether there is even one eigenvalue of the matrix $\mathbf{C} = \mathbf{\Phi}_0(2\pi)$ which satisfies the condition $|\mu_i| > 1$. The results are shown in Fig. A.1. This chart is called the **Ince–Strutt chart** [104, 105]. The shaded area represents unstable parameter sets, and contours represent $\operatorname{tr}\mathbf{C}$. A solid line is used for $\operatorname{tr}\mathbf{C} > 0$, and a dotted line is used for $\operatorname{tr}\mathbf{C} < 0$. It can be seen that curves $\operatorname{tr}\mathbf{C} = \pm 2$ are actually the boundary lines between stable and unstable regions and that bifurcation points of boundary lines appear at

$$\bar{\omega}_0 = \frac{n}{2} \quad (n = 1, 2, 3, \cdots) \ , \tag{A.3.1}$$

where we add a bar above the ω_0 in order to indicate clearly that the value is on the ω_0 axis ($\delta = 0$). The boundaries are called **transition curves**. In the following Appx. A.4, we derive them with a perturbation method.

In Fig. A.2, we concretely selected two points and showed the difference in the behavior of the solution with each parameter sets.

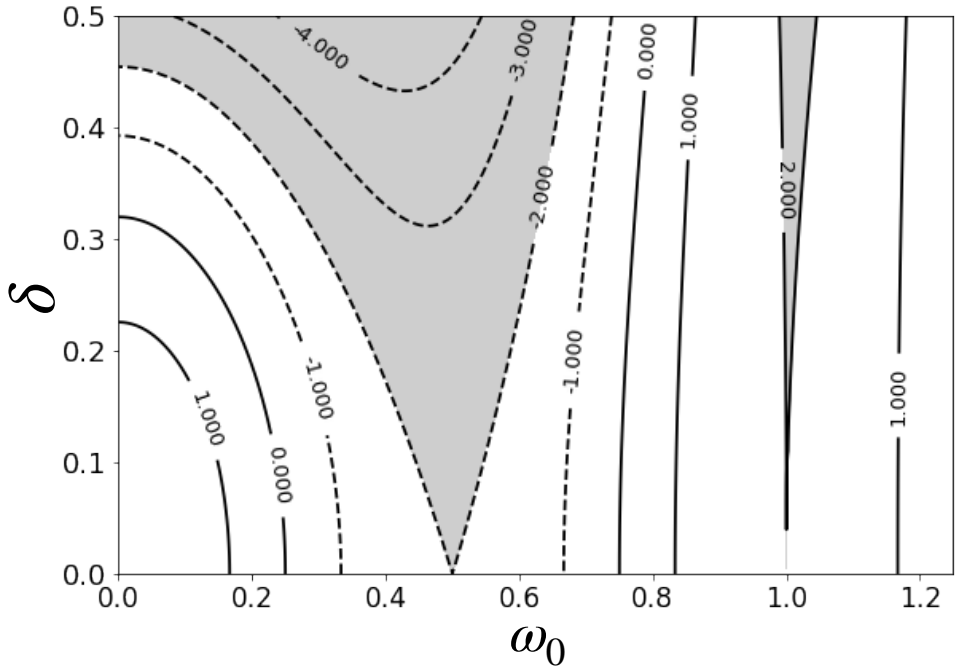

Figure A.1: The Ince–Strutt chart for the Mathieu equation ($\bar{\kappa} = n/2$). The shaded area represents parameter sets which make the solutions of Eq. (A.2.1) unstable. The contour lines of the $\operatorname{tr}\mathbf{C}$ are overlaid. A solid line is used for $\operatorname{tr}\mathbf{C} > 0$, and a dotted line is used for $\operatorname{tr}\mathbf{C} < 0$.

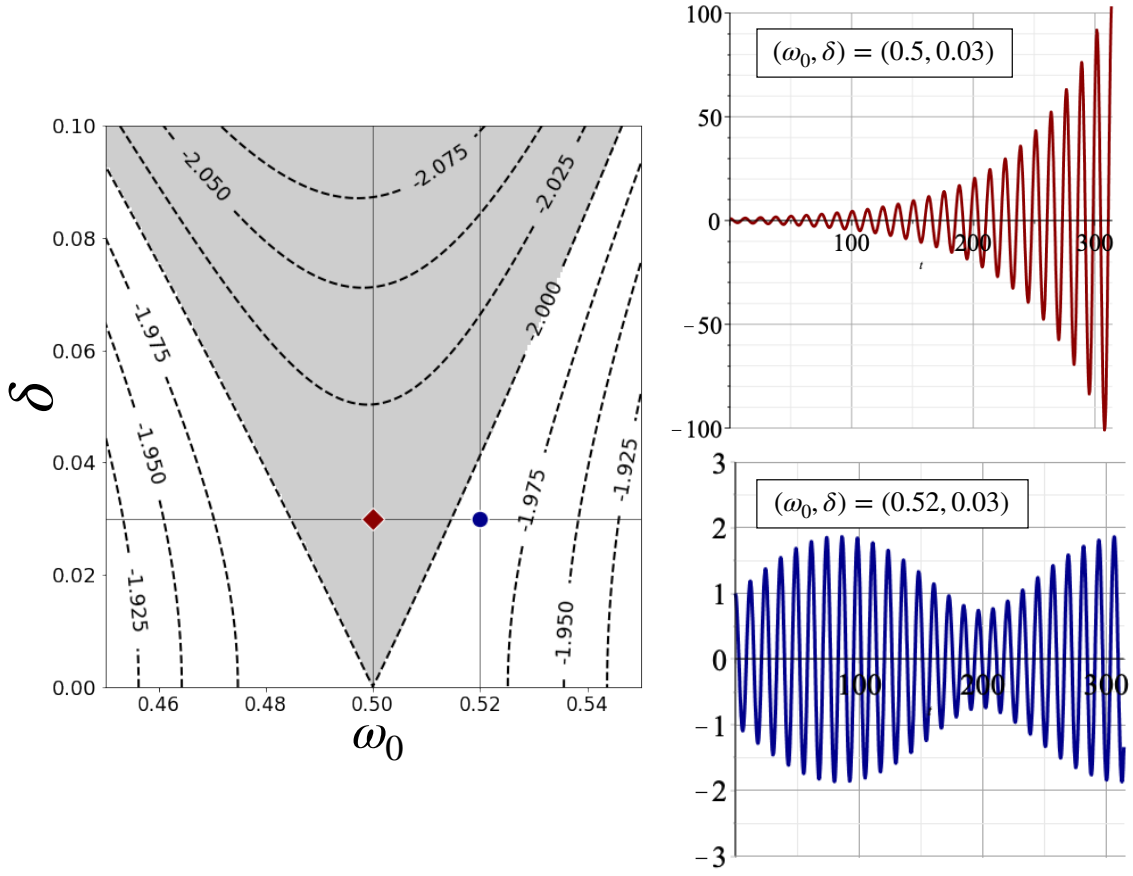

Figure A.2: Left panel : An enlarged view of the area around $\omega_0 = 0.5$ in Fig. A.1. The horizontal line is drawn at the value of $\delta = 0.03$. Right upper panel: An unstable behavior of the solution Eq. (A.2.1). Right lower panel: A bounded and quasi periodic behavior of the solution Eq. (A.2.1).

A.4 Transition Curves

As described in Sec. A.2, the Mathieu equation

$$\ddot{x} + \left[\omega_0^2 + \delta \sin(\tau)\right] x = 0, \tag{A.2.1}$$

has periodic solutions on the transition curves, $\mathrm{tr}\,\mathbf{C} = \pm 2$. In this section, we derive these periodic solutions by treating δ as small values in the case of $\bar{\omega}_0 = 1/2$ and 1. In this process, the concrete expressions of transition curves are obtained.

The equation (A.2.1) can be rewritten as follows:

$$\ddot{x} + \bar{\omega}_0^2 x = -\tilde{\chi} x - \delta \sin(\tau) x \ , \tag{A.4.1}$$

where $\bar{\omega}_0$ is given by Eq. (A.3.1). Here, we introduce small dimensionless parameter $\tilde{\chi}$ and χ, which represent the deviation from normal mode $\bar{\omega}_0$,

$$\omega_0 = \sqrt{\bar{\omega}_0^2 + \tilde{\chi}} = \bar{\omega}_0 + \chi \ . \tag{A.4.2}$$

We assume that the solutions have the following form

$$x(\tau) = x_0(\tau) + x_1(\tau) + x_2(\tau) + \cdots \ , \tag{A.4.3}$$

where $x_i \propto \delta^i$ and $|\delta| \ll 1$. At the same time, ω_0 and $\tilde{\chi}$ are also expanded with δ,

$$\omega_0 = \bar{\omega}_0 + \chi_1 + \chi_2 + \cdots \ , \tag{A.4.4}$$

$$\tilde{\chi} = 0 + \tilde{\chi}_1 + \tilde{\chi}_2 + \cdots \ , \tag{A.4.5}$$

where $\chi_i \propto \delta^i$ and $\tilde{\chi}_i \propto \delta^i$. We solve the equations iteratively.

$$\begin{aligned}
&\ddot{x}_0 + \bar{\omega}_0^2 x_0 = 0, \\
&\ddot{x}_1 + \bar{\omega}_0^2 x_1 = -\tilde{\chi}_1 x_0 - \delta \sin(\tau) x_0, \\
&\ddot{x}_2 + \bar{\omega}_0^2 x_2 = -\tilde{\chi}_1 x_1 - \tilde{\chi}_2 x_0 - \delta \sin(\tau) x_1, \\
&\qquad \vdots
\end{aligned}$$

- $\bar{\omega}_0 = 1/2$

  The equation to be solved is as follows:

$$\ddot{x} + \frac{1}{4}x = -\left(\omega_0^2 - \frac{1}{4}\right)x - \delta \sin(\tau) x = -\tilde{\chi} x - \delta \sin(\tau) x \ . \tag{A.4.6}$$

  First of all, in the case of the zeroth order, we obtain a solution with $T = 4\pi$,

$$x_0(\tau) = c_1 \cos\left(\frac{\tau}{2}\right) + c_2 \sin\left(\frac{\tau}{2}\right) \ . \tag{A.4.7}$$

  Next, the first order equation is given as follows:

$$\begin{aligned}
\ddot{x}_1 + \frac{1}{4}x_1 &= -\tilde{\chi}_1 x_0 - \delta \sin(\tau) x_0 \ , \\
&= \left(-\tilde{\chi}_1 c_1 - \frac{\delta}{2} c_2\right) \cos\left(\frac{\tau}{2}\right) + \left(-\tilde{\chi}_1 c_2 - \frac{\delta}{2} c_1\right) \sin\left(\frac{\tau}{2}\right) \\
&\quad - \frac{\delta}{2}\left[c_1 \sin\left(\frac{3}{2}\tau\right) - c_2 \cos\left(\frac{3}{2}\tau\right)\right] \ .
\end{aligned} \tag{A.4.8}$$

  The first and second terms in the right hand side make the amplitude of the solution increase over time; they are called **secular term**s.
  Since we want to get a periodic solution, we impose the following conditions:

$$\left(-\tilde{\chi}_1 c_1 - \frac{\delta}{2} c_2\right) = 0 \ \text{ and } \ \left(-\tilde{\chi}_1 c_2 - \frac{\delta}{2} c_1\right) = 0 \ . \tag{A.4.9}$$

  Assuming $c_1 \neq 0$ and $c_2 \neq 0$, the following relation is obtained, which are actually boundary lines:

$$\chi_1 = \pm \frac{\delta}{2}, \tag{A.4.10}$$

  where $\chi = \tilde{\chi}$ in the case of $\bar{\omega}_0 = 1/2$.

$$x_1(\tau) = \frac{\delta}{4}\left[c_1 \sin\left(\frac{3}{2}\tau\right) - c_2 \cos\left(\frac{3}{2}\tau\right)\right] \ . \tag{A.4.11}$$

- $\bar{\omega}_0 = 1$

  Similarly, in the case of $\bar{\omega}_0 = 1$, we deal with the following equations,

$$\ddot{x} + x = -\left(\omega_0^2 - 1\right)x - \delta\sin(\tau)x = -\tilde{\chi}x - \delta\sin(\tau)x \ . \tag{A.4.12}$$

  In the zeroth order, there is a solution with $T = 2\pi$,

$$x_0(\tau) = c_1\cos(\tau) + c_2\sin(\tau) \ . \tag{A.4.13}$$

  The first order equation has secular terms again,

$$\ddot{x}_1 + x_1 = -\tilde{\chi}_1[c_1\cos(\tau) + c_2\sin(\tau)] - \frac{\delta}{2}[c_1\sin(2\tau) - c_2\cos(2\tau)] - \frac{\delta}{2}c_2; \tag{A.4.14}$$

  thus, we impose a condition $\tilde{\chi}_1 = 0$,

$$x_1 = \frac{\delta}{6}[c_1\sin(2\tau) - c_2\cos(2\tau)] - \frac{\delta}{2}c_2 \ . \tag{A.4.15}$$

  In order to get the transition curves, it is necessary to consider up to the second order,

$$\begin{aligned}\ddot{x}_2 + x_2 =& c_1\left[-\tilde{\chi}_2 - \frac{\delta^2}{12}\right]\cos(\tau) + c_2\left[-\tilde{\chi}_2 + \frac{5}{12}\delta^2\right]\sin(\tau) \\ &+ \frac{\delta^2}{12}[c_1\cos(3\tau) + c_2\sin(3\tau)] \ .\end{aligned} \tag{A.4.16}$$

  From the condition that secular terms should vanish,

$$\left[-\tilde{\chi}_2 - \frac{\delta^2}{12}\right] = 0 \ \text{ and } \ \left[-\tilde{\chi}_2 + \frac{5}{12}\delta^2\right] = 0 \ , \tag{A.4.17}$$

  we obtain transition curves,

$$\chi_2 = -\frac{\delta^2}{24} \ \text{ and } \ \chi_2 = \frac{5}{24}\delta^2 \ , \tag{A.4.18}$$

  where $\chi = \tilde{\chi}/2$ in the case of $\bar{\omega}_0 = 1$.

$$x_2 = -\frac{\delta^2}{96}[c_1\cos(3\tau) + c_2\sin(3\tau)] \ . \tag{A.4.19}$$

From the above, in the case of $|\delta| \ll 1$, it was found that the width of the unstable region around $\bar{\omega}_0 = 1$ is narrower by about δ than that of around $\bar{\omega}_0 = 1/2$.

Appendix B

Concrete Formulas for Analyzing Transition Curves at $\bar{\kappa} = 3/4$

In this appendix, we give concrete formulas which were not able to be covered in Subsec. 4.4.3. Evaluating the determinant of $R_{3/4}(q, \chi, \beta, \epsilon)$ at the leading order, we can get the following formula,

$$\begin{aligned}&\det[R_{3/4}(q,\chi,\beta,\epsilon)]_{\text{leading}}\\&= \frac{102515625}{262144}\left[q+\frac{9}{25}\left(\chi+\frac{25}{24}\beta^2\right)^2\right]\left[q+\left(\chi-\frac{3}{8}\beta^2-\frac{4}{15}\epsilon^2\right)^2\right]\left[q+\left(\chi-\frac{4}{15}\epsilon^2\right)^2\right].\end{aligned} \tag{B.0.1}$$

The determinant of $R_{3/4}(q,\chi,\beta,\epsilon)$ at the next leading order is given by

$$
\begin{aligned}
&\det[R_{3/4}(q,\chi,\beta,\epsilon)]_{\text{next leading}} \\
&= \left(\frac{16858125\,\epsilon^2}{131072}+\frac{999185625\,\chi}{262144}+\frac{1004653125\,\beta^2}{1048576}\right)q^3 \\
&+\left(-\frac{875255625\,\beta^4\epsilon^2}{16777216}-\frac{157773825\,\epsilon^2\chi^2}{131072}-\frac{1278574875\,\beta^2\epsilon^2\chi}{2097152}-\frac{25022925\,\epsilon^4\chi}{131072}+\frac{4829625\,\beta^2\epsilon^4}{262144}\right. \\
&\left.+\frac{20676718125\,\beta^4\chi}{8388608}+\frac{7811690625\,\beta^6}{67108864}+\frac{2239761375\,\beta^2\chi^2}{1048576}+\frac{2389570875\,\chi^3}{262144}-\frac{155925\,\epsilon^6}{32768}\right)q^2 \\
&+\left(-\frac{55255921875\,\beta^8\epsilon^2}{1073741824}-\frac{256480425\,\epsilon^2\chi^4}{131072}-\frac{41518828125\,\beta^{10}}{1073741824}-\frac{1899828675\,\beta^4\epsilon^2\chi^2}{2097152}\right. \\
&-\frac{1549325475\,\beta^2\epsilon^2\chi^3}{1048576}+\frac{324707990625\,\beta^8\chi}{1073741824}+\frac{22505596875\,\beta^6\epsilon^2\chi}{134217728}+\frac{885060675\,\beta^4\epsilon^4\chi}{16777216} \\
&+\frac{86667165\,\beta^2\epsilon^4\chi^2}{262144}-\frac{154456875\,\beta^6\epsilon^4}{16777216}-\frac{34266645\,\epsilon^4\chi^3}{65536}-\frac{5557987125\,\beta^6\chi^2}{8388608} \\
&+\frac{2187820125\,\beta^4\chi^3}{1048576}+\frac{3551961375\,\beta^2\chi^4}{1048576}+\frac{1781584875\,\chi^5}{262144}-\frac{20585745\,\beta^2\epsilon^6\chi}{524288} \\
&\left.-\frac{19207125\,\beta^4\epsilon^6}{2097152}+\frac{1971783\,\epsilon^6\chi^2}{8192}-\frac{382725\,\beta^2\epsilon^8}{65536}-\frac{168399\,\epsilon^8\chi}{8192}-\frac{2025\,\epsilon^{10}}{2048}\right)q \\
&-\frac{157181056875\,\beta^8\epsilon^2\chi^2}{1073741824}+\frac{52579471275\,\beta^6\chi^3\epsilon^2}{134217728}-\frac{2718276975\,\beta^4\chi^4\epsilon^2}{16777216}-\frac{2757861675\,\beta^2\epsilon^2\chi^5}{2097152} \\
&-\frac{81848475\,\epsilon^2\chi^6}{131072}+\frac{324707990625\,\beta^8\chi^3}{1073741824}-\frac{15516765\,\epsilon^4\chi^5}{131072}-\frac{131274675\,\beta^6\epsilon^4\chi^2}{4194304} \\
&-\frac{557685\,\beta^2\epsilon^4\chi^4}{32768}+\frac{763069815\,\beta^4\chi^3\epsilon^4}{16777216}-\frac{52275587625\,\beta^6\chi^4}{67108864}-\frac{3174157125\,\beta^4\chi^5}{8388608} \\
&+\frac{2316853125\,\chi^6\beta^2}{1048576}+\frac{391199625\,\chi^7}{262144}-\frac{41518828125\,\beta^{10}\chi^2}{1073741824}+\frac{2560977\,\epsilon^6\chi^4}{32768} \\
&-\frac{55647\,\epsilon^8\chi^3}{8192}+\frac{5843390625\,\beta^{10}\epsilon^2\chi}{268435456}+\frac{37858336875\,\beta^8\epsilon^4\chi}{1073741824}+\frac{86993595\,\beta^4\epsilon^6\chi^2}{2097152} \\
&+\frac{51850125\,\beta^6\epsilon^6\chi}{16777216}+\frac{59875443\,\beta^2\epsilon^6\chi^3}{524288}-\frac{877797\,\beta^2\epsilon^8\chi^2}{65536}-\frac{4501575\,\beta^4\epsilon^8\chi}{524288} \\
&-\frac{50625\,\beta^4\epsilon^{10}}{262144}-\frac{729\,\epsilon^{10}\chi^2}{2048}-\frac{1268915625\,\beta^8\epsilon^6}{268435456}-\frac{8758125\,\epsilon^8\beta^6}{4194304} \\
&\left.-\frac{102515625\,\beta^{10}\epsilon^4}{33554432}-\frac{18225\,\beta^2\epsilon^{10}\chi}{32768}\right. .
\end{aligned}
\tag{B.0.2}
$$

A concrete expression for the leading order of discriminant $D_{\text{up to next leading}}$ is given by

$$
\begin{aligned}
&D_{\text{up to next leading}}\left(-\frac{5}{32}\beta^2+\frac{\epsilon^2}{6}+X,\beta,\epsilon\right)\Big|_{\text{leading}}\\
&\quad=\frac{72874359645335178370006084442138671875}{15845632502852867518708790 0672}X^2\beta^{18}\epsilon^2\\
&\qquad+\frac{58039686077603846159926414489746093 75}{19807040628566084398385987584}X^2\beta^{16}\epsilon^4\\
&\qquad+\frac{30577865593094780185718536376953125}{30948500982134506872478 1056}X^2\beta^{14}\epsilon^6\\
&\qquad+\frac{14377122086744872773399353027343 75}{77371252455336267181195264}X^2\beta^{12}\epsilon^8\\
&\qquad+\frac{44660116398490644218444824218 75}{24178516392292583494123 52}X^2\beta^{10}\epsilon^{10}\\
&\qquad+\frac{22902623794097766265869140625}{30223145490365729367654 4}X^2\beta^8\epsilon^{12}\\
&\qquad+\frac{15141672504086309283545708656311035 15625}{50706024009129176059868128215 04}X^2\beta^{20}\\
&\qquad-\frac{63090302100359622014773786067962646484375}{12980742146337069071326240823 05024}\beta^{22}\epsilon^4\\
&\qquad-\frac{30364316518889657654169201850891113281 25}{40564819207303340847894502572032}\beta^{20}\epsilon^6\\
&\qquad-\frac{24183202532334935899969339370727539062 5}{50706024009129176059868128215 04}\beta^{18}\epsilon^8\\
&\qquad-\frac{12740777330456158410716056823730468 75}{79228162514264337593543950336}\beta^{16}\epsilon^{10}\\
&\qquad-\frac{59904675361436969889163970947265625}{19807040628566084398385987584}\beta^{14}\epsilon^{12}\\
&\qquad-\frac{18608381832704435091018676757812 5}{61897001964269013744956211 2}\beta^{12}\epsilon^{14}\\
&\qquad-\frac{95427599142074026107788085937 5}{77371252455336267181195264}\beta^{10}\epsilon^{16}\ .
\end{aligned}
\tag{B.0.3}
$$

Bibliography

[1] R. Durrer and A. Neronov, "*Cosmological magnetic fields: their generation, evolution and observation*," The Astronomy and Astrophysics Review **21**, 62 (2013), arXiv:1303.7121[astro-ph.CO].

[2] K. Subramanian, "*The origin, evolution and signatures of primordial magnetic fields*," Reports on Progress in Physics **79**, 076901 (2016), arXiv:1504.02311[astro-ph.CO].

[3] L. M. Widrow, "*Origin of galactic and extragalactic magnetic fields*," Rev. Mod. Phys. **74**, 775 (2002), arXiv:astro-ph/0207240[astro-ph].

[4] E. García–Berro, M. Kilic, and S. O. Kepler, "*Magnetic white dwarfs: Observations, theory and future prospects*," International Journal of Modern Physics D **25**, 1630005 (2016), arXiv:1510.08676[astro-ph.SR].

[5] A. Y. Potekhin, "*The physics of neutron stars*," Physics-Uspekhi **53**, 1235–1256 (2010), arXiv:1102.5735[astro-ph.SR].

[6] A. Neronov and I. Vovk, "*Evidence for Strong Extragalactic Magnetic Fields from Fermi Observations of TeV Blazars*," Science **328**, 73 (2010), arXiv:1006.3504[astro-ph].

[7] F. Tavecchio *et al.*, "*The intergalactic magnetic field constrained by Fermi/Large Area Telescope observations of the TeV blazar 1ES 0229+200*," Monthly Notices of the Royal Astronomical Society: Letters **406**, L70 (2010), arXiv:1004.1329[astro-ph.CO].

[8] L. Maiani, R. Petronzio, and E. Zavattini, "*Effects of nearly massless, spin-zero particles on light propagation in a magnetic field*," Phys. Lett. B **175**, 359 (1986).

[9] G. Raffelt and L. Stodolsky, "*Mixing of the photon with low-mass particles*," Phys. Rev. D **37**, 1237 (1988).

[10] R. D. Peccei and H. R. Quinn, "CP *Conservation in the Presence of Pseudoparticles*," Phys. Rev. Lett. **38**, 1440 (1977).

[11] R. D. Peccei and H. R. Quinn, "*Constraints imposed by* CP *conservation in the presence of pseudoparticles*," Phys. Rev. D **16**, 1791 (1977).

[12] S. Weinberg, "*A New Light Boson?*," Phys. Rev. Lett. **40**, 223 (1978).

[13] F. Wilczek, "*Problem of Strong P and T Invariance in the Presence of Instantons*," Phys. Rev. Lett. **40**, 279 (1978).

[14] P. Svrcek and E. Witten, "*Axions in string theory*," J. High Energy Phys. **2006**, 051 (2006), arXiv:hep-th/0605206[hep-th].

[15] A. Arvanitaki, S. Dimopoulos, S. Dubovsky, N. Kaloper, and J. March-Russell, "*String axiverse*," Phys. Rev. D **81**, 123530 (2010), arXiv:0905.4720[hep-th].

[16] C. Csáki, N. Kaloper, and J. Terning, "*Effects of the intergalactic plasma on supernova dimming via photon-axion oscillations*," Phys. Lett. B **535**, 33 (2002), arXiv:hep-ph/0112212[hep-ph].

[17] C. Csáki, N. Kaloper, and J. Terning, "*Dimming Supernovae without Cosmic Acceleration*," Phys. Rev. Lett. **88**, 16 (2002), arXiv:hep-ph/0111311[hep-ph].

[18] C. Deffayet, D. Harari, J.-P. Uzan, and M. Zaldarriaga, "*Dimming of supernovae by photon-pseudoscalar conversion and the intergalactic plasma*," Phys. Rev. D **66**, 043517 (2002), arXiv:hep-ph/0112118[hep-ph].

[19] Y. Grossman, S. Roy, and J. Zupan, "*Effects of initial axion production and photon-axion oscillation on type Ia supernova dimming*," Phys. Lett. B **543**, 23 (2002), arXiv:hep-ph/0204216[hep-ph].

[20] M. Christensson and M. Fairbairn, "*Photon–axion mixing in an inhomogeneous universe*," Phys. Lett. B **565**, 10 (2003), arXiv:astro-ph/0207525[astro-ph].

[21] A. De Angelis, M. Roncadelli, and O. Mansutti, "*Evidence for a new light spin-zero boson from cosmological gamma-ray propagation?*," Phys. Rev. D **76**, 121301 (2007), arXiv:0707.4312[astro-ph].

[22] M. Simet, D. Hooper, and P. D. Serpico, "*Milky Way as a kiloparsec-scale axionscope*," Phys. Rev. D **77**, 063001 (2008), arXiv:0712.2825[astro-ph].

[23] M. A. Sánchez-Conde, D. Paneque, E. Bloom, F. Prada, and A. Domínguez, "*Hints of the existence of axion-like-particles from the gamma-ray spectra of cosmological sources*," Phys. Rev. D **79**, 123511 (2009), arXiv:0905.3270[astro-ph.CO].

[24] A. Mirizzi and D. Montanino, "*Stochastic conversions of TeV photons into axion-like particles in extragalactic magnetic fields*," J. Cosmol. Astropart. Phys **2009**, 004 (2009), arXiv:0911.0015[astro-ph.HE].

[25] A. De Angelis, G. Galanti, and M. Roncadelli, "*Relevance of axion-like particles for very-high-energy astrophysics*," Phys. Rev.D **84**, 105030 (2011), arXiv:1106.1132[astro-ph.HE].

[26] D. Horns *et al.*, "*Hardening of TeV gamma spectrum of active galactic nuclei in galaxy clusters by conversions of photons into axionlike particles*," Phys. Rev. D **86**, 075024 (2012), arXiv:1207.0776[astro-ph.HE].

[27] A. De Angelis, G. Galanti, and M. Roncadelli, "*Erratum: Relevance of axion-like particles for very-high-energy astrophysics [Phys. Rev. D 84, 105030 (2011)]*," Phys. Rev. D **87**, 109903 (2013), arXiv:1106.1132[astro-ph.HE].

[28] A. Abramowski *et al.*, "*Constraints on axionlike particles with H.E.S.S. from the irregularity of the PKS 2155-304 energy spectrum*," Phys. Rev. D **88**, 102003 (2013), arXiv:1311.3148[astro-ph.HE].

[29] M. Meyer, D. Montanino, and J. Conrad, "*On detecting oscillations of gamma rays into axion-like particles in turbulent and coherent magnetic fields*," J. Cosmol. Astropart. Phys **2014**, 003 (2014), arXiv:1406.5972[astro-ph.HE].

[30] D. Wouters and P. Brun, "*Anisotropy test of the axion-like particle Universe opacity effect: a case for the Cherenkov Telescope Array*," J. Cosmol. Astropart. Phys **2014**, 016 (2014), arXiv:1309.6752[astro-ph.HE].

[31] D. Harari and P. Sikivie, "*Effects of a Nambu-Goldstone boson on the polarization of radio galaxies and the cosmic microwave background*," Phys. Lett. B **289**, 67 (1992).

[32] P. Jain, S. Panda, and S. Sarala, "*Electromagnetic polarization effects due to axion-photon mixing*," Phys. Rev. D **66**, 085007 (2002), arXiv:hep-ph/0206046[hep-ph].

[33] N. Agarwal, P. Jain, D. W. McKay, and J. P. Ralston, "*Signatures of pseudoscalar photon mixing in CMB polarization*," Phys. Rev. D **78**, 085028 (2008), arXiv:0807.4587[hep-ph].

[34] N. Bassan, A. Mirizzi, and M. Roncadelli, "*Axion-like particle effects on the polarization of cosmic high-energy gamma sources*," J. Cosmol. Astropart. Phys **2010**, 010 (2010), arXiv:1001.5267[astro-ph.HE].

[35] A. Payez, J. R. Cudell, and D. Hutsemékers, "*On the circular polarisation of light from axion–photon mixing*," AIP Conference Proceedings **1241**, 444 (2010), arXiv:0911.3145[astro-ph.CO].

[36] N. Agarwal, A. Kamal, and P. Jain, "*Alignments in quasar polarizations: Pseudoscalar-photon mixing in the presence of correlated magnetic fields*," Phys. Rev. D **83**, 065014 (2011), arXiv:0911.0429[hep-ph].

[37] A. Payez, J. R. Cudell, and D. Hutsemékers, "*Can axionlike particles explain the alignments of the polarizations of light from quasars?*," Phys. Rev. D **84**, 085029 (2011), arXiv:1107.2013[astro-ph.CO].

[38] N. Agarwal *et al.*, "*A complete 3D numerical study of the effects of pseudoscalar–photon mixing on quasar polarizations*," The European Physical Journal C **72**, 1928 (2012), arXiv:1108.3400[astro-ph.CO].

[39] A. Payez, J. Cudell, and D. Hutsemékers, "*New polarimetric constraints on axion-like particles*," J. Cosmol. Astropart. Phys **2012**, 041 (2012), arXiv:1204.6187[astro-ph.CO].

[40] D. Horns, L. Maccione, A. Mirizzi, and M. Roncadelli, "*Probing axionlike particles with the ultraviolet photon polarization from active galactic nuclei in radio galaxies*," Phys. Rev. D **85**, 085021 (2012), arXiv:1203.2184[astro-ph.HE].

[41] A. Payez, "*Constraining ALPs with linear and circular polarisation measurements of quasar light*," (2013), arXiv:1309.6114[astro-ph.CO].

[42] Y. Gong *et al.*, "*Testing the Axion-Conversion Hypothesis of 3.5 keV Emission with Polarization*," Phys. Rev. Lett. **118**, 061101 (2017), arXiv:1612.05697[astro-ph.HE].

[43] E. Masaki, A. Aoki, and J. Soda, "*Stability of axion dark matter-photon conversion*," Phys. Rev. D **101**, 043505 (2020), arXiv:1909.11470[hep-ph].

[44] D. J. Marsh, "*Axion cosmology*," Physics Reports **643**, 1 (2016), arXiv:1510.07633[astro-ph.CO].

[45] M. Kuster, G. Raffelt, and B. Beltrán, "*Axions: Theory, cosmology, and experimental searches*," (Springer, 2007).

[46] P. Sikivie, "*Invisible Axion Search Methods*," Reviews of Modern Physics (2020), arXiv:2003.02206[hep-ph].

[47] L. Di Luzio, M. Giannotti, E. Nardi, and L. Visinelli, "*The landscape of QCD axion models*," Phys. Rept. **870**, 1 (2020), arXiv:2003.01100[hep-ph].

[48] W. A. Bardeen and S.-H. Tye, "*Current algebra applied to properties of the light Higgs boson*," Physics Letters B **74**, 229 (1978).

[49] W. A. Bardeen, R. Peccei, and T. Yanagida, "*Constraints on variant axion models*," Nuclear Physics B **279**, 401 (1987).

[50] M. S. Turner, "*Windows on the axion*," Physics Reports **197**, 67 (1990).

[51] A. Arvanitaki and S. Dubovsky, "*Exploring the string axiverse with precision black hole physics*," Phys. Rev. D **83**, 044026 (2011), arXiv:1004.3558[hep-th].

[52] A. Arvanitaki, M. Baryakhtar, and X. Huang, "*Discovering the QCD axion with black holes and gravitational waves*," Phys. Rev. D **91**, 084011 (2015), arXiv:1411.2263[hep-ph].

[53] G. G. Raffelt, "*Astrophysical methods to constrain axions and other novel particle phenomena*," Physics Reports **198**, 1 (1990).

[54] A. Ayala, I. Domínguez, M. Giannotti, A. Mirizzi, and O. Straniero, "*Revisiting the Bound on Axion-Photon Coupling from Globular Clusters*," Phys. Rev. Lett. **113**, 191302 (2014), arXiv:1406.6053[astro-ph.SR].

[55] J. Ellis and K. Olive, "*Constraints on light particles from supernova SN 1987A*," Physics Letters B **193**, 525 (1987).

[56] G. Raffelt and D. Seckel, "*Bounds on exotic-particle interactions from SN1987A*," Phys. Rev. Lett. **60**, 1793 (1988).

[57] M. S. Turner, "*Axions from SN1987A*," Phys. Rev. Lett. **60**, 1797 (1988).

[58] J. E. Kim, "*Weak-Interaction Singlet and Strong* CP *Invariance*," Phys. Rev. Lett. **43**, 103 (1979).

[59] M. Shifman, A. Vainshtein, and V. Zakharov, "*Can confinement ensure natural CP invariance of strong interactions?*," Nuclear Physics B **166**, 493 (1980).

[60] A. Zhitnitsky, "*On Possible Suppression of the Axion Hadron Interactions (In Russian)*," Sov. J. Nucl. Phys. **31**, 260 (1980).

[61] M. Dine, W. Fischler, and M. Srednicki, "*A simple solution to the strong CP problem with a harmless axion*," Physics Letters B **104**, 199 (1981).

[62] S. L. Cheng, C. Q. Geng, and W.-T. Ni, "*Axion-photon couplings in invisible axion models*," Phys. Rev. D **52**, 3132 (1995).

[63] M. Taoso, G. Bertone, and A. Masiero, "*Dark matter candidates: a ten-point test*," Journal of Cosmology and Astroparticle Physics **2008**, 022 (2008), arXiv:0711.4996[astro-ph].

[64] J. L. Feng, "*Dark Matter Candidates from Particle Physics and Methods of Detection*," Ann. Rev. Astron. Astrophys. **48**, 495 (2010), arXiv:1003.0904[astro-ph.CO].

[65] T. Lin, "*Dark matter models and direct detection*," PoS **333**, 009 (2019), arXiv:1904.07915[hep-ph].

[66] F. Zwicky, "*Spectral displacement of extra galactic nebulae*," Helv. Phys. Acta **6**, 110–127 (1933).

[67] V. C. Rubin and J. Ford, W. Kent, "*Rotation of the Andromeda Nebula from a Spectroscopic Survey of Emission Regions*," Astrophysical Journal **159**, 379 (1970).

[68] V. C. Rubin, J. Ford, W. K., and N. Thonnard, "*Rotational properties of 21 SC galaxies with a large range of luminosities and radii, from NGC 4605 (R=4kpc) to UGC 2885 (R=122kpc).*," Astrophysical Journal **238**, 471 (1980).

[69] N. Aghanim *et al.*, "*Planck 2018 results. VI. Cosmological parameters*," Astron. Astrophys. **641**, 67 (2020), arXiv:1807.06209[astro-ph.CO].

[70] J. Preskill, M. B. Wise, and F. Wilczek, "*Cosmology of the invisible axion*," Physics Letters B **120**, 127 (1983).

[71] L. Abbott and P. Sikivie, "*A cosmological bound on the invisible axion*," Physics Letters B **120**, 133 (1983).

[72] M. Dine and W. Fischler, "*The not-so-harmless axion*," Physics Letters B **120**, 137 (1983).

[73] E. W. Kolb and M. S. Turner, "*The Early Universe*," (Addison-Wesley Publishing Compay, 1990).

[74] L. Hui, J. P. Ostriker, S. Tremaine, and E. Witten, "*Ultralight scalars as cosmological dark matter*," Phys. Rev. D **95**, 043541 (2017), arXiv:1610.08297[astro-ph.CO].

[75] J. I. Read, "*The local dark matter density*," Journal of Physics G: Nuclear and Particle Physics **41**, 063101 (2014), arXiv:1404.1938[astro-ph.GA].

[76] S. J. Asztalos *et al.*, "*Experimental Constraints on the Axion Dark Matter Halo Density*," The Astrophysical Journal **571**, L27 (2002), arXiv:astro-ph/0104200[astro-ph].

[77] R. Kato and J. Soda, "*Search for ultralight scalar dark matter with NANOGrav pulsar timing arrays*," Journal of Cosmology and Astroparticle Physics **2020**, 036 (2020), arXiv:1904.09143[astro-ph.HE].

[78] V. Anastassopoulos *et al.*, "*New CAST limit on the axion–photon interaction*," CAST, Nature Physics **13**, 584 (2017), arXiv:1705.02290[hep-ex].

[79] P. Sikivie, "*Experimental Tests of the "Invisible" Axion*," Phys. Rev. Lett. **51**, 1415 (1983).

[80] P. Sikivie, "*Detection rates for "invisible"-axion searches*," Phys. Rev. D **32**, 2988 (1985).

[81] P. Sikivie, "*Erratum: Detection rates for "invisible"-axion searches*," Phys. Rev. D **36**, 974 (1987).

[82] T. Braine *et al.*, "*Extended Search for the Invisible Axion with the Axion Dark Matter Experiment*," Phys. Rev. Lett. **124**, 101303 (2020), arXiv:1910.08638[hep-ex].

[83] A. Caldwell *et al.*, "*Dielectric Haloscopes: A New Way to Detect Axion Dark Matter*," Phys. Rev. Lett. **118**, 091801 (2017), arXiv:1611.05865[physics.ins-det].

[84] P. Brun *et al.*, "*A new experimental approach to probe QCD axion dark matter in the mass range above 40 μeV*," The European Physical Journal C **79**, 186 (2019), arXiv:1901.07401[physics.ins-det].

[85] J. L. Ouellet *et al.*, "*First Results from ABRACADABRA-10 cm: A Search for Sub-μeV Axion Dark Matter*," Phys. Rev. Lett. **122**, 121802 (2019), arXiv:1810.12257[hep-ex].

[86] K. Ehret *et al.*, "*New ALPS results on hidden-sector lightweights*," Physics Letters B **689**, 149 (2010), arXiv:1004.1313[hep-ex].

[87] R. Ballou *et al.*, "*New exclusion limits on scalar and pseudoscalar axionlike particles from light shining through a wall*," Phys. Rev. D **92**, 092002 (2015), arXiv:1506.08082[hep-ex].

[88] R. Bähre *et al.*, "*Any light particle search II — Technical Design Report*," Journal of Instrumentation , T09001 (2013), arXiv:1302.5647[physics.ins-det].

[89] M. Gertsenshtein, "*Wave resonance of light and gravitional waves*," Journal of Experimental and Theoretical Physics **14**, 84 (1962).

[90] E. Masaki and J. Soda, "*Conversion of gravitons into dark photons in cosmological dark magnetic fields*," Phys. Rev. D **98**, 023540 (2018), arXiv:1804.00458[astro-ph.CO].

[91] F. Wilczek, "*Two applications of axion electrodynamics*," Phys. Rev. Lett. **58**, 1799 (1987).

[92] E. Masaki, A. Aoki, and J. Soda, "*Photon-axion conversion, magnetic field configuration, and polarization of photons*," Phys. Rev. D **96**, 043519 (2017), arXiv:1702.08843[astro-ph.CO].

[93] S. Das *et al.*, "*Probing light pseudoscalars with light propagation, resonance and spontaneous polarization*," J. Cosmol. Astropart. Phys **2005**, 002 (2005), arXiv:hep-ph/0408198[hep-ph].

[94] S. Das *et al.*, "*The dynamical mixing of light and pseudoscalar fields*," Pramana **70**, 439 (2008), arXiv:hep-ph/0410006[hep-ph].

[95] C. Wang and D. Lai, "*Axion-photon propagation in magnetized universe*," J. Cosmol. Astropart. Phys **2016**, 006 (2016), arXiv:1511.03380[astro-ph.HE].

[96] D. Yoshida and J. Soda, "*Electromagnetic waves propagating in the string axiverse*," Progress of Theoretical and Experimental Physics **2018** (2018), arXiv:1710.09198[hep-th].

[97] D. Espriu and A. Renau, "*Photons in a cold axion background and strong magnetic fields: Polarimetric consequences*," International Journal of Modern Physics A **30**, 1550099 (2015), arXiv:1401.0663[hep-ph].

[98] N. W. McLachlan, "*Theory and application of Mathieu functions*," (Dover Publications, 1965).

[99] I. Kovacic, R. Rand, and S. Mohamed Sah, "*Mathieu's Equation and Its Generalizations: Overview of Stability Charts and Their Features*," Applied Mechanics Reviews **70**, 020802 (2018).

[100] D. W. Jordan and S. Peter, "*Nonlinear ordinary differential equations: an introduction for scientists and engineers*," (Oxford University Press, 2007).

[101] R. H. Rand, "*Lecture Notes on Nonlinear Vibrations*," (Cornell University Library) .

[102] G. Floquet, "*Sur les équations différentielles linéaires à coefficients périodiques*," Annales scientifiques de l'École Normale Supérieure **12**, 47 (1883).

[103] E. Mathieu, "*Mémoire sur le mouvement vibratoire d'une membrane de forme elliptique*," Journal de Mathématiques Pures et Appliquées **13**, 137 (1868).

[104] E. Ince, "*IV.–Researches into the Characteristic Numbers of the Mathieu Equation*," Proceedings of the Royal Society of Edinburgh **46**, 20 (1927).

[105] M. J. O. Strutt, "*Zur Wellenmechanik des Atomgitters*," Annalen der Physik **391**, 319 (1928).